J. metamorphic Geol., 1991, **9**, 315–332

Infiltration-driven dehydration and anatexis in granulite facies metagabbro, Grenville Province, Ontario, Canada

D. R. M. PATTISON
Department of Geology and Geophysics, University of Calgary, Calgary, Alberta, T2N-1N4, Canada

ABSTRACT Dark hornblende + garnet-rich, quartz-absent metagabbro boudins from the Seguin subdomain, Ontario Grenville Province, are transected by anastomosing light-coloured veins rich in orthopyroxene, clinopyroxene, plagioclase and sometimes quartz. The veins vary in texture from fine-grained diffuse veins and patches that overprint the metagabbro, to coarse tonalitic leucosomes with sharp borders. The diffuse veins and patches are suggestive of channellized subsolidus dehydration of the metagabbro, while the tonalitic leucosomes are suggestive of local internally-derived anatexis. All vein types grade smoothly into each other, with the tonalitic leucosomes being the latest.

Relative to the host metagabbro, the veins have higher Si, Na, Ba & Sr, lower Fe, Mg, Ca & Ti, and similar Al. The coarser veins are enriched in K. Plagioclase becomes steadily enriched in Na in the transition from host metagabbro (An_{47}) to the veins (An_{35}), and in the coarsest veins it is antiperthitic. Differences in composition of the other minerals between host metagabbro and vein are minor. Pressure–temperature estimates are scattered, but indicate a minimum temperature during vein formation of 700° C at about 8 kbar.

Mass balance constraints indicate that the veins formed from the metagabbro in an open system. The transecting veins are interpreted to represent pathways of Si + Na + Ba + Sr ± K ± Al-enriched, low a_{H_2O} fluids that metasomatized the host metagabbro to form the anhydrous veins. An initial period of localized solid-state dehydration of the metagabbro, represented by the diffuse veins, was followed by a transition to localized anatexis, represented by the tonalitic leucosomes. The change to anatexis may have been due to the addition of K to the infiltrating fluid. The source and delivery mechanism of the fluids is unknown.

Key words: anatexis; dehydration; granulite; Grenville Province; infiltration; low a_{H_2O}; metagabbro.

INTRODUCTION

One of the most intriguing aspects of granulite formation is the relationship between fluid movement, dehydration and anatexis in the middle and lower crust. Of particular interest are studies conducted on mixed granulite–amphibolite rocks, in which hydrous amphibolite facies rocks are transected by veins and patches of anhydrous mineralogy characteristic of the granulite facies. Bradshaw (1989) investigated garnet-bearing quartzo-feldspathic veins that transect two-pyroxene granulites in the Lower Cretaceous Fiordland terrane of New Zealand. He ascribed the formation of the veins to solid-state dehydration of the host rock triggered by infiltration of carbonic fluids. Metasomatism accompanied dehydration: Bradshaw argued that garnet stability was favoured by lowered whole rock $Fe^{2+}/(Fe^{2+} + Fe^{3+})$ and Na caused by fluid passage.

Hansen *et al.* (1987) and Stahle *et al.* (1987) investigated charnockitic patches that transect biotite + amphibole-bearing tonalitic gneiss in the amphibolite–granulite transition of the southern Indian Precambrian shield. They concluded that solid-state dehydration of amphibole-bearing gneiss to form orthopyroxene-bearing charnockite was caused by infiltration of carbonic fluids along ductile shears and foliation planes, a conclusion proposed earlier by Newton *et al.* (1980). As in the New Zealand veins, metasomatism accompanied dehydration, as shown by increases in K, Na, Si, Ba & Sr and decreases in Ca, Fe, Mg, Ti & Y in the charnockite relative to the gneiss.

In the same area, the Closepet Granite has its roots in the vicinity of the amphibolite–granulite transition (Friend, 1981). Friend (1983) investigated the textural and structural relationships between features characteristic of CO_2-infiltration (charnockitic patches) and features characteristic of incipient anatexis (quartzo-feldspathic segregations and dykes). Based on the close relationships between the different types of features, he suggested that infiltration of fluids was responsible for both processes: introduced CO_2-rich fluids dehydrated and metasomatized the tonalitic gneiss to produce charnockite, during which process the fluids took on K and H_2O, making them agents of anatexis. By extrapolation, he speculated that the magma for the Closepet Granite was formed by such infiltration-driven metasomatism.

The present study is an investigation of the relationships between infiltration-driven dehydration and anatexis in metabasic granulite from the Grenville Province, Ontario.

The rocks concerned are remarkable single outcrops of hornblende-rich, quartz-absent metagabbro cross-cut by a network of pyroxene + plagioclase-rich veins. Contrasting modal mineralogy and textures in the veins suggest that the veins formed by *both* subsolidus and anatectic processes. The close spatial and textural relationships between different vein types suggest that they were formed during an episode of infiltration by low-a_{H_2O} fluids. A scenario is proposed in which chemical changes in the introduced fluid resulted in a transition from localized subsolidus dehydration of the metagabbro to localized anatexis.

DEHYDRATION, MELTING AND DEHYDRATION-MELTING

The qualitative relationships between anatexis, subsolidus dehydration and variable a_{H_2O} may be illustrated with isobaric T–a_{H_2O} diagrams (Greenwood, 1975; Powell, 1983; Grant, 1985; Waters, 1988). Corresponding P–T and T–a_{H_2O} diagrams for selected reactions involving hornblende (Hbd), quartz (Qtz), orthopyroxene (Opx), clinopyroxene (Cpx), plagioclase (Pl), silicate liquid (L) and vapour (V) in the system CaO–MgO–Al_2O_3–SiO_2–H_2O (CMASH) are illustrated schematically in Fig. 1. Reactants and products are appropriate for tschermakitic hornblende and the liquid compositions determined experimentally by Ellis & Thompson (1986).

For simplicity, singular points (e.g. Grant, 1986) and multi-variancy of the reactions are not considered. It is further assumed that as a_{H_2O} decreases in a mixed vapour, the stability field of coexisting melt also decreases (in contrast, see Peterson & Newton, 1989a).

Three main types of reaction may be considered.

(1) Dehydration reactions, for example Hbd + Qtz = Opx + Cpx + Pl + V, in which H_2O from the breakdown of hornblende is released as a free vapour phase. Melt is not involved.

(2) Vapour-consuming melting reactions, for example Hbd + Pl + Qtz + V = Cpx + L and Opx + Pl + Qtz + V = Cpx + L, in which melting consumes any free vapour. In vapour-consuming melting reactions, the major reactants volumetrically are plagioclase, quartz and vapour, which combine to form the quartzo-feldspathic melt. The solidus of the system is defined by reactions of this type (Fig. 1a). In general, production of melt by these reactions is minor unless a_{H_2O} is externally buffered (Powell, 1983).

(3) Dehydration melting reactions (Thompson, 1982), for example Hbd + Qtz = Opx + Cpx + Pl + L, in which water released from the breakdown of hornblende is dissolved directly into the melt phase. To balance the production of quartzo-feldspathic melt from the breakdown of hornblende + quartz, there is substantial production of pyroxene. Dehydration-melting reactions may proceed under vapour-absent or vapour-present conditions

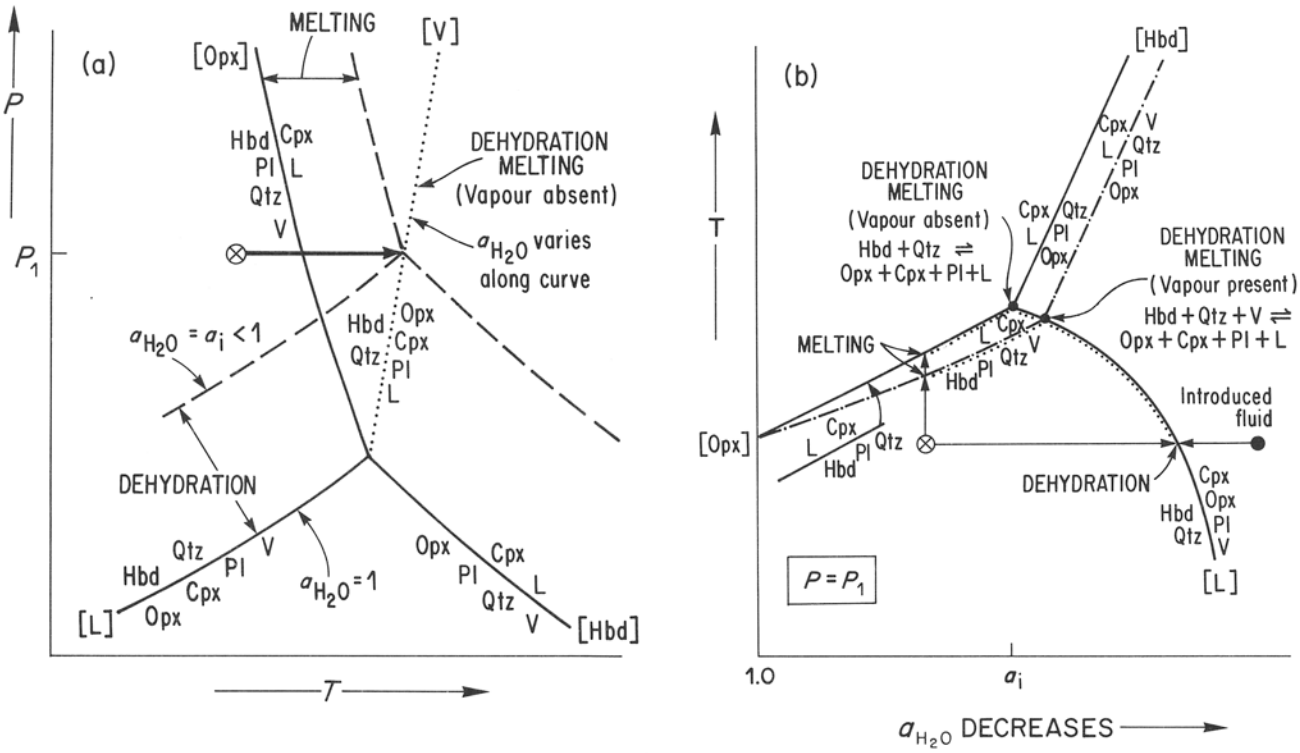

Fig. 1. Schematic P–T (a) and T–a_{H_2O} (b) diagrams showing the relationships between melting and dehydration reactions involving hornblende (Hbd), quartz (Qtz), clinopyroxene (Cpx), orthopyroxene (Opx), plagioclase (Pl), silicate liquid (L), and vapour (V). Open circle with cross represents on arbitrary P–T–a_{H_2O} starting condition (see discussion in text). Solid circle is an arbitrary introduced fluid composition.

(e.g. Peterson & Newton, 1989b; Fig. 1b). For clarity, only the vapour-absent dehydration-melting reaction is illustrated in Fig. 1(a).

The main disadvantage of the P–T diagram is that it can only portray relationships for fixed a_{H_2O}. This is particularly disadvantageous for granulite facies rocks, which have been shown in numerous studies to have variable and low a_{H_2O} (e.g. Phillips, 1980; Hansen *et al.*, 1984; Lamb & Valley, 1984). In particular, a_{H_2O} along the vapour-absent dehydration-melting reaction Hbd + Qtz = Opx + Cpx + Pl + L (dotted line in Fig. 1a) decreases from a value of 1.0 (at the H_2O-saturated invariant point) to lower values with increasing pressure. Consequently, this reaction on a P–T diagram represents the *projection* onto the P–T plane of a *line* in P–T–a_{H_2O} space. In contrast, the other reactions (solid lines in Fig. 1a) represent the *intersection* at some fixed a_{H_2O} of the P–T plane with *planar* reaction surfaces in P–T–a_{H_2O} space.

In a number of high-grade terranes, the amphibolite–granulite facies transition is marked by little or no pressure difference (e.g. Broken Hill, Australia, Phillips, 1980; Namaqualand, South Africa, Waters, 1988). In these instances, pressure can be omitted as an important variable, allowing for the application of isobaric T–a_{H_2O} diagrams. The schematic isobaric T–a_{H_2O} diagram in Fig. 1(b) corresponds to $P = P_1$ from the P–T diagram in Fig. 1(a). Reaction curves in the P–T diagram correspond to those in the T–a_{H_2O} diagram, with the exception of the dotted vapour-absent dehydration-melting reaction, which in the T–a_{H_2O} diagram is represented by an isobaric invariant point (fixed for a given pressure). In the P–T diagram, the position of the same reactions for some value of a_{H_2O} less than 1.0 (a_i) is shown by the dashed lines. In the T–a_{H_2O} diagram, dot-dash reactions (Fig. 1b) are for the situation where vapour is always present, becoming progressively more enriched in non-H_2O components (e.g. CO_2) as a_{H_2O} decreases. Finite solubility of CO_2 in silicate melts (Grant, 1985; Peterson & Newton, 1989a) results in the onset of melting reactions at lower temperatures in the presence of a mixed vapour than in the vapour-absent condition.

In the T–a_{H_2O} diagram, the influence of a_{H_2O} on the stability of dehydration and melting reactions can be clearly shown (Powell, 1983). For a given temperature, a typical amphibolite will be in equilibrium with an a_{H_2O} somewhere in the hornblende + quartz stability field, such as indicated in Fig. 1(b). With a temperature increase, the melting reaction Hbd + Pl + Qtz ± V = Cpx + L will be intersected. Because of the small pore volume of high-grade rocks, the amount of melt produced will be negligible (nil in the vapour-absent case). As temperature rises, a_{H_2O} will be internally buffered along the appropriate melting curve to lower values until the corresponding invariant point is reached. At this point, *dehydration melting* will take place by either of the reactions Hbd + Qtz = Opx + Cpx + Pl + L or Hbd + Qtz + V = Opx + Cpx + Pl + L, where there will be substantial production of both melt and pyroxene.

Conversely, starting again from the Hbd + Qtz stability field, subsolidus *dehydration* can only occur if a low-a_{H_2O} fluid is introduced. As the rock and introduced fluid equilibrate with each other, a_{H_2O} of the fluid initially in the hornblende field will shift to lower values, while the externally introduced fluid will shift to higher a_{H_2O} by mixing with the water produced from the breakdown of hornblende to pyroxenes and plagioclase. Provided hornblende + quartz persist, the rock will continue to buffer the fluid composition throughout infiltration; otherwise, a_{H_2O} of the external fluid will be imposed on the rock. If fluid infiltration ceases before hornblende + quartz are consumed, a rise in temperature will result in a_{H_2O} being internally buffered to higher values along the dehydration curve until the appropriate invariant point is reached, where dehydration melting will proceed as before.

LOCATION AND REGIONAL SETTING

The metagabbros of this study are found in road cuttings on either side of Highway 11 immediately south of the junction of Highway 141, about 15 km south of Huntsville, Ontario (Fig. 2). The rocks are part of the Seguin lithotectonic subdomain of the Central Gneiss Belt (CGB) western Grenville Province (Davidson & Grant, 1986, and references therein). The Seguin subdomain is a gently SE-plunging synformal lobe, bounded by shallowly inward-dipping tectonite zones, that overlies the adjacent Rosseau, Parry Sound, Novar and Huntsville lithotectonic subdomains (Davidson *et al.*, 1982; Fig. 2b). The main rock type of the Seguin subdomain is a layered amphibolite facies quartzo-feldspathic migmatitic gneiss, which encloses masses of charnockitic and granodioritic orthogneiss and small bodies of mafic granulite (Nadeau, 1985). Dating of charnockitic gneiss in the Seguin subdomain gives an age range of 1500–1400 Ma. The bounding tectonite zones are interpreted as ductile shear zones which accommodated NW-directed thrusting of the Seguin subdomain over the adjacent subdomains during the evolution of the CGB (Davidson *et al.*, 1982).

Metagabbro bodies are found in clusters and in isolated masses throughout the CGB (Davidson & Grant, 1986). Although they typically have tectonic boundaries, the clustering of the bodies suggests that may not have been transported tectonically very far (A. Davidson, pers. comm.). Many of the metagabbros show primary igneous textures and retain some of the primary gabbroic mineralogy (e.g. olivine), but all have been recrystallized to varying extents. Grant (1988) has described the evolution of the coronitic metagabbros.

Primary baddeleyite and metamorphic zircon coronas around baddeleyite have been dated in a number of coronitic metagabbros in the CGB, including one body in the Seguin subdomain about 40 km northwest of the study area (Davidson & van Breemen, 1988). The baddeleyite gives an average age of *c.* 1170 Ma, about 125 Ma older than the 1045-Ma age of the zircon overgrowths. Davidson & van Breemen interpret the older age to be the igneous

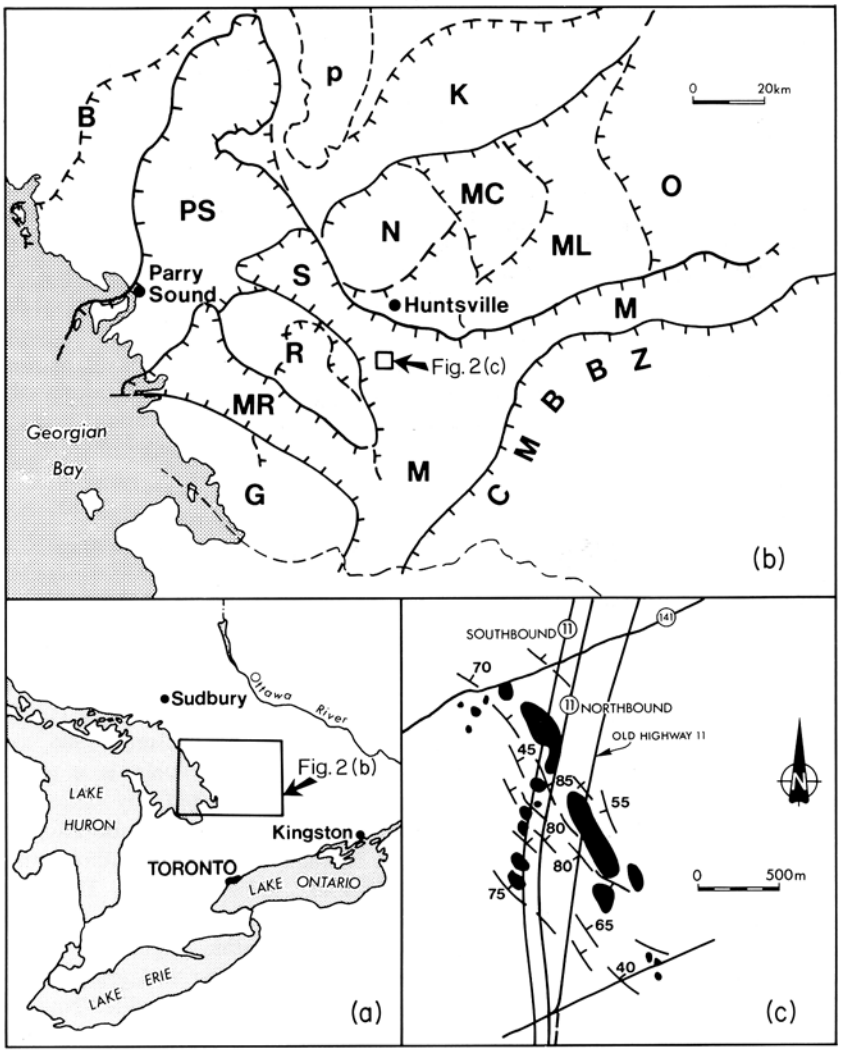

Fig. 2. Location maps for net-veined metagabbros. (a) Southwestern Ontario. (b) Lithotectonic subdivisions of a portion of the Central Gneiss Belt, from Davidson & Grant (1986). B = Britt, CMBBZ = Central Metasedimentary Belt boundary zone. G = Go Home, K = Kiosk, M = Muskoka, MC = McCraney, ML = McLintock, MR = Moon River, N = Novar, O = Opeongo, p = Powassan batholithic complex, PS = Parry Sound, R = Rosseau, S = Seguin. (c) Distribution of metagabbro boudins in the neck of the Seguin Subdomain (modified from Grant, 1987). Lines with dips show the attitude of foliation in the quartzo-feldspathic gneiss that encloses the boudins.

crystallization age and the younger age to be the age of metamorphic recrystallization.

DESCRIPTION OF METAGABBROS

The metagabbros occur as a cluster of boudins in the neck of the Seguin subdomain (Fig. 2c). The boudins vary in area from a few tens of square metres to a maximum size of *c.* $100 \times 500\ m^2$. They are typically equant to pod-shaped and are separated and wrapped by foliated amphibolite facies quartzo-feldspathic gneiss. The interiors of the metagabbros are generally massive, in contrast to the margins, which are well-foliated amphibolite. All contacts with the quartzo-feldspathic gneiss are tectonic. The enclosing gneisses are hornblende + biotite migmatites of generally granodioritic composition, with about 20–30% leucosome and 70–80% mesosome (terminology of Johannes, 1983).

Three main types of metagabbro are found in the interiors of the bodies. Type 1, the rarest of the three and only found in isolated pods and masses in the centre of the largest body, is a relatively anhydrous rock of millimetre–centimetre-sized green clinopyroxene, red garnet and white plagioclase, with or without minor ilmenite, hornblende and orthopyroxene. A distinct igneous texture is preserved, in which the garnet has partially replaced former plagioclase laths. In thin section, the clinopyroxene crystals are intimately intergrown with plagioclase in a sieve texture, and may have a thin rim of hornblende.

Type 2 metagabbro comprises the majority of the bodies. It is a medium-grained hornblende + garnet + plagioclase + clinopyroxene ± biotite ± orthopyroxene metabasite that does not preserve any igneous texture. The boundary between Type 1 and Type 2 metagabbro may be gradational, but is most typically sharply defined. Whole-rock chemical analyses of the two types of metagabbro (Table 1) are similar except for higher TiO_2 and $FeO/(FeO + MgO)$ in Type 1 metagabbro. The difference may be partly explained by higher modal ilmenite in Type 1 metagabbro. The presence in Type 2 metagabbro of relict sieve-textured clinopyroxene crystals, partly replaced by hornblende, suggests that Type 2 metagabbro may in some instances be the variably hydrated and recrystallized equivalent of ilmenite-poorer Type 1 metagabbro. Some loss of Na and gain of K may have accompanied hydration. Alternatively, the two types of metagabbro may represent primary differences upon crystallization of a heterogeneous gabbro.

The third type of metagabbro, which is the particular focus of this study, is a mixed rock in which anastomosing, light-coloured plagioclase + orthopyroxene + clinopyroxene veins and patches transect dark hornblende-rich metabasite (Figs 3 & 4). In some bodies, the veins enclose relatively equant cores of hornblende-rich metabasite, but in others the vein network and mafic cores

Table 1. Whole-rock analyses.

	Type I metagabbro	Type II metagabbro*	Hu1 dark	Hu1 light	Hu1 leucosome	P2-6-2b dark	P2-6-2b light	Hu11-6 dark	Hu11-6 light	Mixed light & dark†
SiO_2	44.03	44.51	44.95	53.26	71.87	44.08	65.15	44.81	67.23	49.26
TiO_2	4.35	1.99	1.78	1.24	0.20	1.92	0.70	1.83	0.56	1.54
Al_2O_3	14.05	14.82	15.21	15.31	15.43	15.58	13.86	15.59	15.14	15.26
FeO	14.89	14.36	13.62	10.06	1.22	14.62	5.79	14.06	4.49	11.69
MnO	0.22	0.23	0.23	0.16	0.02	0.26	0.08	0.24	0.06	0.18
MgO	6.33	8.26	7.25	5.64	0.64	7.84	3.55	7.75	2.44	6.79
CaO	10.20	10.86	10.54	7.83	3.21	11.11	4.71	10.41	4.77	9.68
Na_2O	3.20	2.26	2.44	3.26	4.69	2.03	3.37	2.03	3.53	3.10
K_2O	0.06	0.35	1.07	0.96	1.77	0.98	1.37	1.01	1.03	1.03
P_2O_5	0.30	0.20	0.42	0.30	0.04	0.44	0.17	0.44	0.11	0.37
Total	97.63	97.84	97.51	98.02	99.09	98.86	98.75	98.44	99.36	98.90
LOI	1.05	1.95	1.63	1.08	0.61	1.63	0.67	1.48	0.52	1.30
CO_2	0.18	0.27	0.30	0.31	0.53	0.18	0.22	0.23	0.29	0.23
S	0.11	0.05	0.12	0.11	n.d.	0.14	0.12	0.12	0.14	0.12
V	766	n.a.	303	232	27	296	152	306	95	266
Cr	196	n.a.	363	342	235	511	301	421	362	272
Ni	108	n.a.	47	39	9	54	30	52	31	42
Zn	115	n.a.	127	112	18	128	81	136	61	120
Rb	7	n.a.	23	46	20	25	35	22	18	33
Sr	226	n.a.	198	340	1210	201	686	285	948	352
Y	41	n.a.	46	25	n.d.	49	5	46	n.d.	35
Zr	152	n.a.	182	134	31	188	82	180	62	141
Ba	63	n.a.	336	644	341	403	857	442	699	474
FeO/(FeO + MgO)	0.70	0.63	0.65	0.64	0.66	0.65	0.62	0.64	0.65	0.63
CaO/(CaO + FeO)	0.41	0.43	0.44	0.44	0.72	0.43	0.45	0.43	0.51	0.45
$TiO_2/(TiO_2 + FeO)$	0.23	0.12	0.12	0.11	0.14	0.12	0.11	0.12	0.11	0.12

Oxides are in wt%, trace elements in $\mu g/g$. n.d. = not detected, n.a. = not analysed. All Fe calculated as FeO.
* Average of four samples.
† Average of two samples containing both dark and light domains.

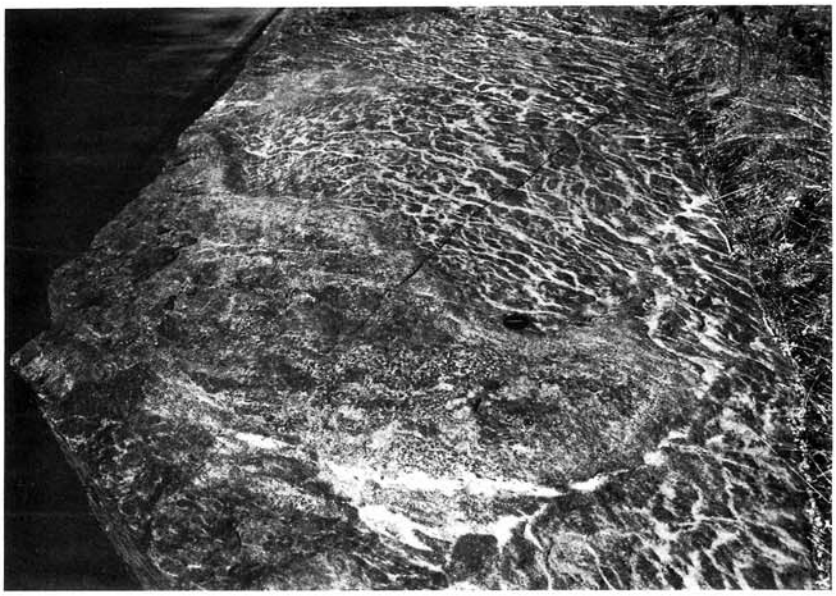

Fig. 3. Surface of outcrop of net-veined metagabbro. Note the pattern of anastomosing light-coloured veins transecting dark metagabbro. Lens cap for scale.

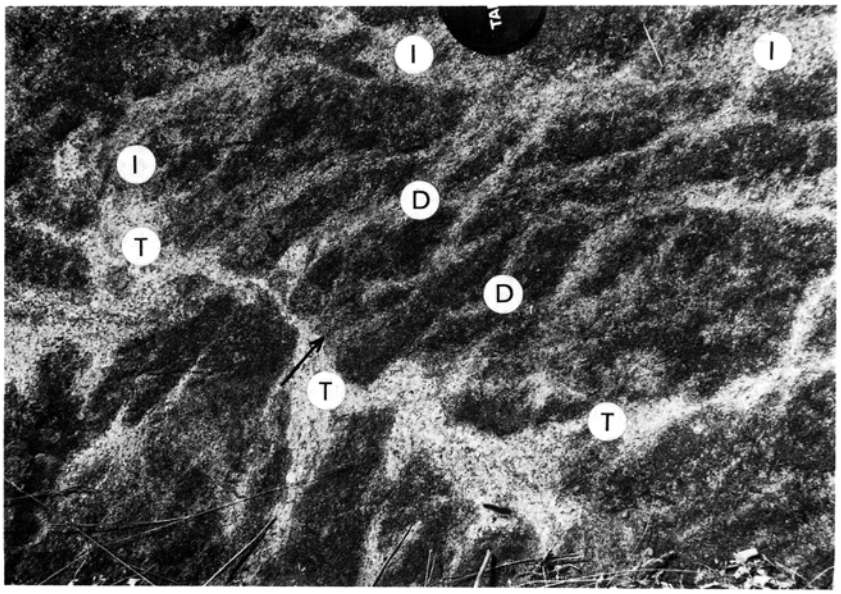

Fig. 4. Illustration of vein types. *Diffuse veins and patches* (D), are characterized by gradational contacts with the dark host metagabbro. *Coarse tonalitic leucosome* (T) is characterized by coarse grain size, quartz + plagioclase-rich composition and sharp margins against the host metagabbro. *Intermediate veins* (I) are similar to the diffuse veins but coarser, wider and more leucocratic. All gradations between vein types can be seen. The tonalitic leucosome appears to be the latest of the vein types, judging by its sharp margins against host metagabbro and diffuse veins (arrow).

have been flattened and folded. The planar fabrics in the flattened bodies form high angles with the foliation in the enclosing quartzo-feldspathic gneisses, indicating that the veins were formed and deformed prior to the incorporation of the metagabbros into the gneiss. The modal mineralogy of light and dark domains in three net veined metagabbros is given in Table 2.

Host metagabbro

The dark metabasite in between the veins contains 40–60% hornblende, which sometimes occurs in poikiloblasts several centimetres in length. In thin section, the hornblende poikiloblasts occur as aggregates of hornblende subgrains, 0.5–1 mm in diameter. Plagioclase, garnet, minor biotite and variable amounts of clinopyroxene (1–13%) are intergrown with the hornblende, along with accessory pyrrhotite, ilmenite and apatite (see 'dark' domains, Table 2). A significant proportion of the clinopyroxene crystals have a sieve texture and are surrounded by hornblende; this texture resembles that described in Type 2 metagabbro. Minor amounts of orthopyroxene are found in the dark domains, increasing in abundance as the light-coloured veins are approached. Quartz is absent.

Veins

The light-coloured veins can be divided into three main kinds, although all gradations between the three are found (Figs 4–7).

Diffuse veins and patches

These are the narrowest and most cryptic type of veins, and they grade smoothly into the host amphibolite (Figs 4 & 5). They vary in width from 0.5 to 1.5 cm. The veins are equigranular, with grain size typically 0.3–0.5 mm. The diffuse margins of these veins contrast markedly with the sharper margins developed between

Table 2. Modal mineralogy.

	Hu1 dark	Hu1 light (1)	Hu1 light (2)	Hu1 leucosome	Hu1 selvage	P2-6-2b dark	P2-6-2b light	Hu15a dark	H15a light
n	1617	1180	2152	1481	1507	3925	2895	2476	2400
Amph	55.8	26.9	19.1	0.0	1.2	38.9	7.3	60.9	10.3
Grt	4.0	1.0	0.6	0.0	0.6	8.6	0.3	8.6	0.0
Cpx	1.3	11.9	11.6	0.0	1.1	12.6	14.9	3.3	15.5
Opx	4.5	10.3	11.8	0.8	17.8	4.9	13.5	1.4	11.2
Bt	3.1	0.1	2.1	3.0	7.7	3.1	1.8	1.1	0.1
Pl	29.5	47.8	48.5	67.8	62.0	30.2	55.9	22.9	56.5
Qtz	0.0	0.0	4.4	28.4	7.6	0.0	4.4	0.0	5.0
Ilm	0.4	0.8	0.9	0.0	0.8	0.4	0.9	0.5	0.4
Py	tr.	tr.	tr.	0.0	0.1	tr.	tr.	0.2	tr.
Po	0.4	0.2	0.3	0.0	0.7	0.4	0.3	0.6	0.4
Ap	0.9	0.6	0.7	0.1	0.3	0.8	0.7	0.6	0.6

n = number of points counted, tr. = <0.1 vol.% of that mineral. 'Dark' refers to the more amphibole-rich host rock; 'light' refers to the more plagioclase-rich veins; 'leucosome' refers to the cross-cutting quartzo-feldspathic leucosome in Hu1; 'selvage' refers to the Bt + Opx-enriched selvage between the leucosome and the amphibolite-rich host rocks in Hu1. Modes were obtained using the electron microprobe point-counting technique of Nicholls & Stout (1986).

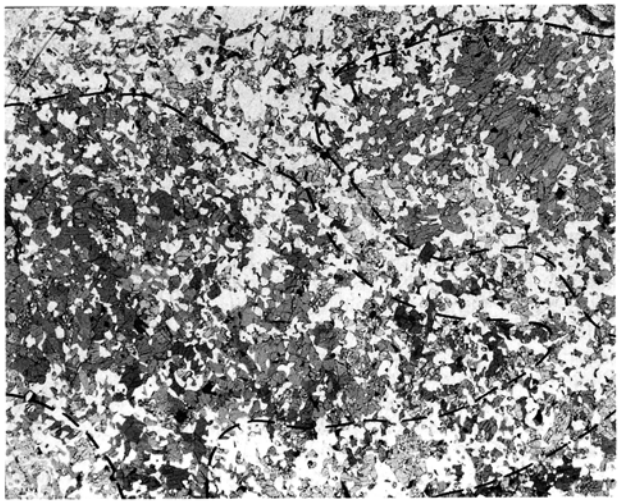

Fig. 5. Sample Hu1. Detail of diffuse pyroxene-rich patches in amphibole-rich metagabbro. The host metagabbro, outlined by dashed lines, comprises (in order of modal abundance) hornblende, plagioclase, garnet, clinopyroxene ± orthopyroxene. The veins comprise (in order of modal abundance) plagioclase, clinopyroxene, orthopyroxene, hornblende and biotite. Note the gradational transition from the hornblende-rich domain to the pyroxene + plagioclase-rich domain (vein), and the dispersed anhedral pyroxene crystals in the vein. Width of photographs in Figs 5–7 = 1.9 cm.

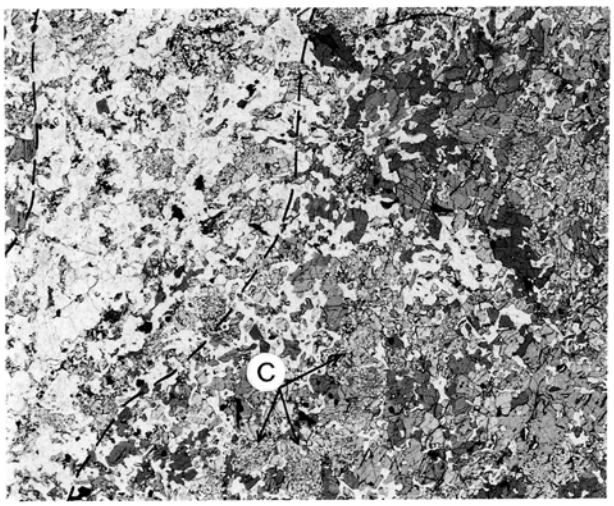

Fig. 6. Sample P2-6-2b. Detail of plagioclase + pyroxene-rich intermediate vein (left) in hornblende + garnet + clinopyroxene-rich host metagabbro. Compared to the diffuse veins in Fig. 5, note the greater width and coarseness of the vein and the more leucocratic mineralogy (which includes antiperthitic plagioclase + quartz). Dark edges of orthopyroxene crystals and polycrystalline aggregates in the vein are thin coatings of pyrite. In the host metagabbro, note the occurrence of poikiloblastic clinopyroxene crystals (C) surrounded by hornblende; these may be remnants from an anhydrous precursor.

leucosomes and mesosomes in anatectic migmatites (e.g. Johannes, 1988).

The minerals consist of plagioclase, clinopyroxene, orthopyroxene and minor biotite, ilmenite, pyrrhotite and apatite, along with remnants of hornblende and garnet from the host amphibolite (see 'Hu1 light', Table 2). Quartz may or may not be present. Orthopyroxene occurs in subidiomorphic crystals and crystal aggregates, sometimes partly replacing isolated hornblende crystals; in some samples it has a fine coating of pyrite along subgrain boundaries. Clinopyroxene occurs in two habits: in subidiomorphic crystals and polycrystalline aggregates, and more rarely in poikiloblastic sieve-textured crystals similar in appearance to those in the host amphibolite and Type 1 and 2 metagabbros; it may be that the latter type of clinopyroxene is a remnant from the host amphibolite. Commonly, orthopyroxene and clinopyroxene occur together.

Plagioclase occurs in twinned equant, subidiomorphic crystals. Quartz, where present, occurs in the centres of the veins in isolated, large (0.5–3.0 mm) grains with undulatory extinction. Quartz rarely is found in contact with hornblende, usually being separated by orthopyroxene or plagioclase. Biotite is typically less abundant and finer grained in the veins than in the host amphibolite. Pyrrhotite grains in the veins sometimes show partial replacement by pyrite at their margins.

In the transition from host amphibolite to the diffuse veins, hornblende usually decreases in abundance and is sometimes replaced by one or both pyroxenes at its margins (Fig. 8). Garnet crystals decrease in size and abundance, and may be surrounded by plagioclase moats.

Intermediate veins

Intermediate veins are similar in texture to the diffuse veins and patches, but are wider (up to 3 cm across), more continuous and coarser (Figs 4 & 6). They contain less amphibole and more quartz than the diffuse veins (see P2-6-2b light and Hu15a light, Table 2). In thin section, the main differences from the diffuse veins are the ubiquitous presence of quartz and the development of antiperthitic plagioclase. The wider veins contain a higher proportion of antiperthitic plagioclase, which is not found in the veins unless quartz is also present in the same vein. It typically occurs in the centres of the veins, usually separated from the hornblende-bearing host assemblage by non-antiperthitic plagioclase. The antiperthitic plagioclase occurs in larger (0.5–1.0 mm) grains than the non-antiperthitic plagioclase, and it may have ragged edges, sometimes with fine (0.1 mm) subgrain development at its margins. The proportion of exsolved K-feldspar in the antiperthite ranges from <1 to 20%, averaging 10–15% (visual estimates).

Quartz, like antiperthite, is always found in the centre of the veins, sometimes in trains of isolated crystals (in two dimensions) that are optically continuous; this texture is similar to that of coarse quartz crystals found in the centres of some pegmatites (Mehnert, 1968). Although normally without inclusions, quartz may contain orthopyroxene, clinopyroxene, biotite and plagioclase crystals. In some samples, quartz is bordered by a vague selvage of orthopyroxene ± biotite. These textures suggest that quartz was in equilibrium with the whole vein assemblage, and is not part of some unrelated early or late quartz vein.

Coarse leucosomes

These veins are the widest (up to 5 cm in width), coarsest grained and most leucocratic (Figs 4 & 7). In contrast to the other vein types, they have relatively sharp margins against both the host amphibolite and more diffuse veins, and thus texturally resemble discrete leucosomes in anatectic migmatites. Sometimes a selvage of orthopyroxene and biotite separates the coarse leucosomes from the hornblende-bearing host (Fig. 7). In addition to antiperthitic texture, the plagioclase in the leucosome may show myremykitic intergrowth with quartz.

Modal mineralogy for the coarse leucosome and its associated

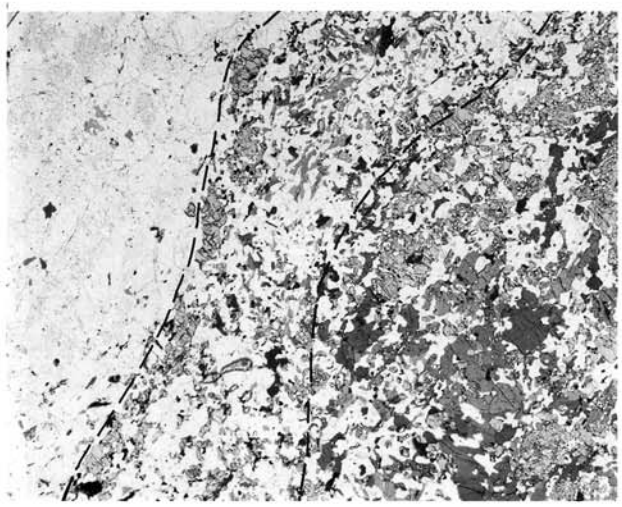

Fig. 7. Sample Hu1. Detail of coarse tonalitic leucosome (left), orthopyroxene + biotite-enriched selvage (centre) and hornblende + garnet + clinopyroxene-rich host metagabbro (right). In contrast to the diffuse and intermediate veins, note the virtual absence of ferromagnesian minerals in the tonalitic leucosome.

selvage are given under Hu1 'leucosome' and Hu1 'selvage' in Table 2. In the leucosome, of the 67.8% plagioclase in the mode, 7.5% represents exsolved K-feldspar in the antiperthitic plagioclase (11.1% exsolution). The volumetrically minor mafic component includes biotite and orthopyroxene. The approximate 68:28 ratio of plagioclase to quartz corresponds to tonalite (Streckeisen classification).

Textural interpretation

The three types of light-coloured veins grade into one another (Fig. 4). Coarse tonalitic leucosome grades smoothly into less sharply defined intermediate veins, which in turn grade smoothly into diffuse patches and veins. These textures suggest that the different veins were produced internally within the host metagabbro by a similar process. The coarse leucosomes are probably the latest of the vein types, as in places they cross-cut diffuse veins (Fig. 4).

Textural contrasts between vein types are suggestive of different modes of formation. The coarse grain size, sharp margins, tonalitic composition and myremykitic textures of the coarse leucosomes suggest that they are crystallized melts that developed locally within the metagabbro. The diffuse veins and patches, in contrast, show none of the above features characteristic of anatexis: they show a smooth textural and mineralogical transition into the host hornblende-rich metagabbro. In the veins, relict crystals of hornblende, sieve-textured clinopyroxene and rarely garnet from the host metagabbro occur in a matrix of orthopyroxene, clinopyroxene, plagioclase and biotite (Fig. 5). Thus, the diffuse veins and patches may be better explained as products of subsolidus conversion of the hornblende + garnet-rich metagabbro to the vein mineralogy.

The intermediate veins show features of both of the above vein types, and may represent a transition from solid-state processes to anatexis. The restriction of quartz + antiperthitic plagioclase to the centres of the intermediate veins suggests that these may represent sites of incipient anatexis, in which the small volume of tonalitic melt produced may have been insufficient to allow segregation.

WHOLE-ROCK CHEMICAL ANALYSES

Whole-rock chemical analyses for three different net veined specimens are listed in Table 1. To separate the relatively diffuse light and dark domains, the samples were sliced into 5-mm slabs and the light and dark domains broken apart. Major and trace element analyses were performed on fused beads and pressed powder pellets, respectively, on an automated wavelength-dispersive Philips PW-1440 X-ray fluorescence spectrometer with a rhodium tube at The University of Calgary (see Sevigny, 1987, for details of methods and analytical uncertainties). Sulphur and carbon analyses were performed on a LECO S-32 analyser and LECO inductance furnace with WR-12 determinator, respectively, at the Institute of Sedimentary and Petroleum Geology, Calgary.

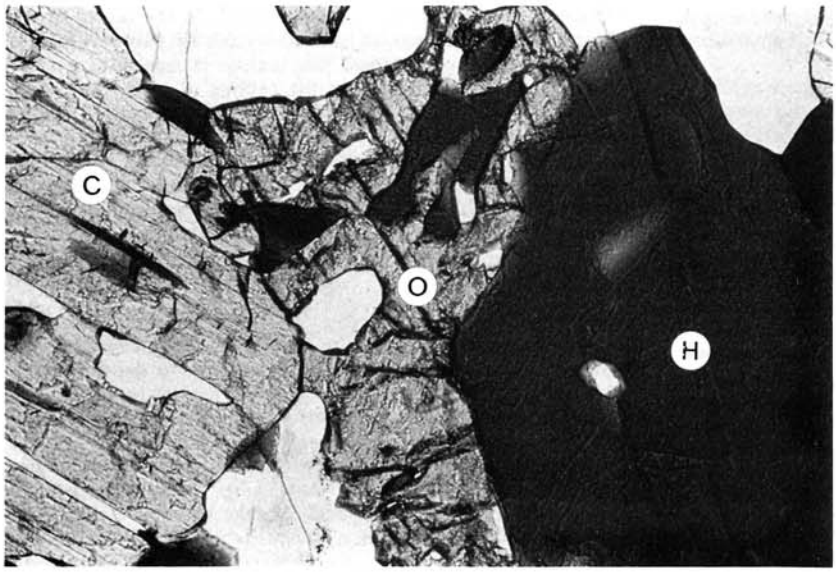

Fig. 8. Anhedral orthopyroxene (O) on the margin of a hornblende crystal (H), adjacent to clinopyroxene (C). In the orthopyroxene, note the enveloped hornblende relicts that are in optical continuity with the main hornblende crystal. Width of photograph = 0.9 mm.

In Table 1, all Fe is calculated as FeO. In analyses of coronitic metagabbro from the Grenville Province, Davidson & van Breemen (1988) report that 19–23% of Fe occurs as Fe_2O_3, which may be taken as an estimate here.

The analyses of the host metagabbro domains ('dark') in the three specimens are similar both to one another and to analyses of homogeneous Type 2 metagabbro. This suggests that the dark hornblende-rich domains in between the light-coloured veins represent essentially unmodified Type 2 metagabbro. Combined with the relict clinopyroxene textures noted above, these data suggest that Type 2 metagabbro may be the protolith to the net-veined metagabbro.

Relative to the host metagabbro, the veins are significantly higher in Si and Na, and lower in Fe, Mn, Mg, Ca, and Ti; Al is about the same. *K* shows no consistent pattern, but is significantly higher in the coarser veins and tonalitic leucosome. There is slightly more CO_2 in the veins. For trace elements, the veins are higher in Ba & Sr, and lower in V, Y, Cr, Ni, Zn & Zr; Rb shows no consistent pattern. These changes are similar to those reported by Hansen *et al.* (1987) and Stahle *et al.* (1987) for transecting charnockitic veins in biotite + amphibole-bearing quartzo-feldspathic gneiss from southern India. Bulk analyses of net-veined metagabbros (veins plus host rock; Table 1) show 20–30% of the same enrichments and depletions relative to the host metagabbro as do the veins, which is consistent with the approximate 1:3 ratio of veins to host in these mixed samples.

The major element variations reflect the higher proportion of quartz and more sodic plagioclase and the lower proportion of ferromagnesian minerals in the veins. The lower modal abundance of ferromagnesian minerals, in particular hornblende, is reflected in the lower V, Y, Cr, Ni & Zn. The increase in Sr & Ba reflects the higher proportion of feldspar in the veins. The irregular behaviour of K & Rb probably reflects the variable abundance of biotite in the veins relative to the host metagabbro. However, in the veins which contain antiperthitic plagioclase, K is higher.

Because the dark hornblende-rich domains are essentially isochemical in major elements with the unveined Type 2 metagabbro, this suggests that the Si + Na + Ba + Sr ± K-enriched veins could not have been derived from the metagabbro in a closed system. It is uncertain if the decreases in Fe, Mg, Ca & Ti in the veins relative to the host metagabbro represent actual losses, or simply dilution by the added Si & Na. Evidence in support of dilution is the relative uniformity of the ratios $FeO/(FeO + MgO)$, $CaO/(CaO + FeO)$ and $TiO_2/(FeO + TiO_2)$ between veins and host metagabbro. If dilution predominated, then to account for no proportionate decrease in Al in the veins, some Al must also have been introduced.

MINERAL CHEMICAL ANALYSES

Chemical analyses of minerals from three net-veined specimens are listed in Table 3. The analyses were performed on the automated wavelength-dispersive ARL-SEMQ electron microprobe at The University of Calgary. Data were reduced according to the procedures of Bence & Albee (1968) and Albee & Ray (1970). Operating conditions were: accelerating voltage of 15 kV; beam current of 0.15 mA; beam diameter of 1.0–1.5 μm; and counting time of 20 s. Typical detection limits and analytical precision for major elements are given in Nicholls & Stout (1988). Detection limits and precision for F in biotite and amphibole are 0.05 and 0.04; for Cl they are 0.01 and <0.01.

In each specimen, groups of coexisting minerals were analysed in the most hornblende-rich part of the host metagabbro ('dark'), in the veins ('light'), and on the margin between the light and dark domains ('margin'). Hu1 contains both diffuse veins and coarse leucosome and specimens P2-6-2b and Hu15a contain intermediate veins. Analysed minerals have uniform compositional profiles up to 50 μm of the rims. Reported analyses are from the centres of the minerals.

$Fe^{3+}/(Fe^{2+} + Fe^{3+})$ ratios

The presence of ilmenite + pyrrhotite ± pyrite and absence of magnetite in all samples suggests that the rocks were fairly reduced (c. QFM). Estimates of Fe^{3+} in garnet are based on the relation $Fe^{3+} = 2.0 - Al^{VI}$, giving an average $Fe^{3+}/(Fe^{2+} + Fe^{3+})$ of 0.03. For pyroxenes, Fe^{3+} was estimated from the relation $Al^{IV} + Na = Al^{VI} + 2Ti + Fe^{3+}$ (Papike *et al.*, 1974, cited in Lindsley, 1983), giving average $Fe^{3+}/(Fe^{2+} + Fe^{3+})$ ratios of 0.05 for orthopyroxene and 0.09 for clinopyroxene. In amphiboles, estimated $Fe^{3+}/(Fe^{2+} + Fe^{3+})$ ratios average 0.21 for the '13eNK' calculation scheme and 0.11 for the average of the '15eNK' and '13eCNK' calculation schemes of Robinson *et al.* (1982) (calculations performed using the AMPHIBOL program of L. R. Richard & D. B. Clarke, Department of Geology, Dalhousie University, Halifax). $Fe^{3+}/(Fe^{3+} + Fe^{2+})$ estimates were not performed for biotite.

Amphibole

The amphibole in the host metagabbro and the veins can be classified as a ferroan pargasite (Leake, 1978). It is slightly more tschermakitic than amphibole in Type 2 (unveined) metagabbro (e.g. $Na_{0.78}K_{0.18}Ca_{1.89}Fe_{1.77}Mg_{2.47}Ti_{0.28}Al_{2.54}Si_{6.00}O_{22}(F_{0.04}Cl_{0.14})(OH, O)_n$).

Clinopyroxene

Clinopyroxene has a wider range of composition in a given rock than the other ferromagnesian minerals. This variability reflects to some extent the textural distinction between irregularly-shaped crystals that are typical of clinopyroxene associated with vein formation, and the poikiloblastic sieve-textured crystals that may be relicts from the anhydrous precursor to the host metagabbro. The chemical data in Table 3 are for the non-poikiloblastic type of clinopyroxene. In contrast, typically sieve-textured clinopyroxene contains less Ca (for example, in P2-6-2b, $Na_{0.05}Ca_{0.82}Mg_{0.70}Fe_{0.37}Al_{0.15}Si_{1.92}$). This is similar to clinopyroxene in Type 1 metagabbro ($Na_{0.10}Ca_{0.82}Mg_{0.71}Fe_{0.29}Al_{0.14}Si_{1.94}$) and to clinopyroxenes in coronitic metagabbros reported by Grant (1988), supporting the textural evidence that the sieve-textured clinopyroxenes may be relict.

Plagioclase

Plagioclase decreases in X_{Ca} in the transition from the host metagabbro to the veins. In hornblende-rich metagabbro, X_{Ca} is typically 0.46. In non-antiperthitic plagioclase, X_{Ca} ranges from 0.39 in the diffuse veins to 0.35 in the intermediate veins. In antiperthitic plagioclase, X_{Ca} of the host plagioclase ranges from 0.31 in the intermediate veins to 0.27 in the tonalitic leucosome.

K-feldspar exsolution lamellae in the antiperthitic plagioclase are enriched in Ba (*c.* 1.0–1.8 wt%, corresponding to 0.02–0.03 cations). Integrating the K-feldspar exsolution lamellae with the host plagioclase gives a pre-exsolution plagioclase composition of $Ca_{0.242}Na_{0.636}K_{0.121}$ in the tonalitic leucosome of Hu1 (11.1% exsolution).

Compositional differences between veins and host metagabbro

Apart from plagioclase, there are only slight differences in mineral composition between the veins and the host metagabbro. Relative to the host metagabbro, in the veins there are small decreases in: $Mg/(Mg + Fe)$ in coexisting ferromagnesian minerals (0.01–0.05); Al in hornblende (0.04–0.13) and the two pyroxenes (0.0–0.05); and Na in hornblende (0.02–0.04). There are small increases in Ba in biotite (0.01–0.02).

Table 3. Mineral analyses.

	Hu1 dark	Hu1 margin	Hu1 light	Hu1 leucosome	P2-6-2b dark	P2-6-2b margin	P2-6-2b light	Hu15a dark	Hu15a light
					Garnet (12 oxygens)				
SiO_2	37.71	37.53	—	—	38.33	38.17	—	38.31	—
Al_2O_3	21.06	21.07	—	—	21.29	21.59	—	21.33	—
TiO_2	0.03	0.00	—	—	0.02	0.04	—	0.04	—
FeO	27.90	27.53	—	—	26.06	25.52	—	27.96	—
MnO	1.80	2.05	—	—	0.99	1.17	—	2.03	—
MgO	5.12	4.72	—	—	6.17	5.66	—	4.95	—
CaO	6.39	6.60	—	—	7.06	7.94	—	6.39	—
Total	100.01	99.50	—	—	99.92	100.09	—	101.01	—
Si	2.98	2.98	—	—	2.99	2.98	—	2.99	—
Al	1.96	1.97	—	—	1.96	1.99	—	1.96	—
Fe	1.84	1.83	—	—	1.70	1.67	—	1.83	—
Mn	0.12	0.14	—	—	0.07	0.08	—	0.13	—
Mg	0.60	0.56	—	—	0.72	0.66	—	0.58	—
Ca	0.54	0.56	—	—	0.59	0.66	—	0.53	—
Mg/(Mg + Fe)	24.6	23.4	—	—	29.7	28.3	—	24.0	—
$Fe^{2+}/(Fe^{3+} + Fe^{2+})$	0.035	0.027	—	—	0.029	0.023	—	0.026	—
					Amphibole (23 oxygens)				
SiO_2	40.52	39.93	40.82	—	40.52	40.88	—	40.74	40.83
Al_2O_3	12.61	12.72	11.90	—	13.05	12.16	—	12.35	12.12
TiO_2	2.49	2.55	2.21	—	2.22	2.61	—	2.49	2.70
FeO	16.90	17.31	17.77	—	15.47	16.03	—	16.67	17.42
MnO	0.15	0.11	0.16	—	0.08	0.12	—	0.16	0.14
MgO	9.79	9.56	9.31	—	10.56	10.10	—	9.88	9.20
CaO	11.33	11.32	11.32	—	11.42	11.36	—	11.30	11.32
BaO	0.05	0.10	0.04	—	0.01	0.05	—	0.12	0.07
Na_2O	1.51	1.44	1.41	—	1.67	1.59	—	1.67	1.52
K_2O	1.79	1.87	1.77	—	1.70	1.73	—	1.60	1.68
F	0.10	0.12	0.13	—	0.16	0.15	—	0.12	0.09
Cl	0.09	0.09	0.10	—	0.03	0.03	—	0.06	0.06
Total	97.33	97.13	97.06	—	96.90	96.86	—	97.21	97.22
Si	6.18	6.13	6.27	—	6.16	6.24	—	6.22	6.25
Al	2.27	2.30	2.16	—	2.34	2.19	—	2.22	2.19
Ti	0.29	0.29	0.26	—	0.25	0.30	—	0.29	0.31
Fe	2.16	2.22	2.28	—	1.97	2.05	—	2.13	2.23
Mn	0.02	0.01	0.02	—	0.01	0.02	—	0.02	0.02
Mg	2.23	2.19	2.13	—	2.39	2.30	—	2.25	2.10
Ca	1.85	1.86	1.86	—	1.86	1.86	—	1.85	1.86
Na	0.45	0.43	0.42	—	0.49	0.47	—	0.47	0.45
K	0.35	0.37	0.35	—	0.33	0.34	—	0.31	0.33
F	0.05	0.06	0.06	—	0.08	0.07	—	0.06	0.04
Cl	0.02	0.02	0.03	—	0.01	0.01	—	0.02	0.02
Mg/(Mg + Fe)	50.8	49.6	48.3	—	54.9	52.9	—	51.4	48.5
$Fe^{3+}/(Fe^{3+} + Fe^{2+})$	0.117	0.145	0.105	—	0.121	0.084	—	0.111	0.077
					Clinopyroxene (6 oxygens)				
SiO_2	51.67	—	52.45	—	50.93	51.82	51.69	51.15	51.53
Al_2O_3	2.70	—	2.42	—	3.19	2.64	2.09	2.21	1.82
TiO_2	0.24	—	0.22	—	0.28	0.29	0.20	0.19	0.20
FeO	10.81	—	11.40	—	10.39	10.66	11.44	10.87	11.29
MnO	0.28	—	0.27	—	0.16	0.26	0.18	0.27	0.30
MgO	11.96	—	11.77	—	12.41	12.33	12.34	12.29	11.98
CaO	21.88	—	21.89	—	21.41	21.90	21.33	21.46	21.55
Na_2O	0.55	—	0.56	—	0.62	0.60	0.62	0.56	0.58
Total	100.09	—	100.98	—	99.39	100.50	99.89	99.00	99.25
Si	1.94	—	1.96	—	1.92	1.94	1.95	1.95	1.96
Al	0.12	—	0.11	—	0.14	0.12	0.09	0.10	0.08
Ti	0.01	—	0.00	—	0.01	0.01	0.01	0.01	0.01
Fe	0.34	—	0.36	—	0.33	0.33	0.36	0.35	0.36
Mn	0.01	—	0.01	—	0.01	0.01	0.01	0.01	0.01
Mg	0.67	—	0.65	—	0.70	0.69	0.69	0.70	0.68
Ca	0.88	—	0.88	—	0.87	0.88	0.86	0.88	0.88
Na	0.04	—	0.04	—	0.05	0.04	0.05	0.04	0.04
Mg/(Mg + Fe)	66.4	—	64.8	—	68.0	67.3	65.8	66.8	65.4
$Fe^{3+}/(Fe^{3+} + Fe^{2+})$	0.047	—	0.042	—	0.119	0.096	0.105	0.110	0.117

Table 3. (*Continued*)

	Hu1 dark	Hu1 margin	Hu1 light	Hu1 leucosome	P2-6-2b dark	P2-6-2b margin	P2-6-2b light	Hu15a dark	Hu15a light
					Orthopyroxene (6 oxygens)				
SiO_2	51.02	50.91	51.07	51.67	50.85	50.98	50.57	50.68	50.39
Al_2O_3	1.42	1.15	1.44	1.01	1.54	1.39	1.21	1.10	1.09
TiO_2	0.04	0.04	0.07	0.06	0.07	0.07	0.08	0.07	0.05
FeO	28.45	29.31	29.41	25.63	27.17	27.63	28.95	29.31	29.70
MnO	0.68	0.75	0.70	0.45	0.44	0.47	0.49	0.73	0.69
MgO	18.61	18.07	17.59	20.61	19.97	18.92	18.66	18.22	17.72
CaO	0.42	0.43	0.47	0.34	0.39	0.42	0.49	0.44	0.48
Total	100.64	100.66	100.75	99.77	100.43	99.88	100.45	100.55	100.12
Si	1.95	1.95	1.96	1.96	1.93	1.95	1.94	1.95	1.95
Al	0.06	0.05	0.07	0.05	0.07	0.06	0.06	0.05	0.05
Fe	0.91	0.94	0.94	0.81	0.86	0.89	0.93	0.94	0.96
Mn	0.02	0.02	0.02	0.02	0.01	0.02	0.02	0.02	0.02
Mg	1.06	1.03	1.00	1.17	1.13	1.08	1.07	1.04	1.02
Ca	0.02	0.02	0.02	0.01	0.02	0.02	0.02	0.02	0.02
Mg/(Mg + Fe)	53.8	52.4	51.6	58.9	56.7	55.0	53.5	52.6	51.5
$Fe^{3+}/(Fe^{3+} + Fe^{2+})$	0.044	0.047	0.027	0.041	0.075	0.037	0.059	0.053	0.052
					Biotite (11 oxygens)				
SiO_2	35.72	35.63	35.00	36.43	—	34.41	—	35.20	—
Al_2O_3	15.00	14.91	14.77	14.84	—	14.84	—	14.79	—
TiO_2	5.75	5.79	5.78	5.76	—	5.95	—	5.83	—
FeO	18.38	19.64	19.94	16.88	—	18.04	—	18.54	—
MnO	0.04	0.07	0.11	0.06	—	0.09	—	0.05	—
MgO	11.22	10.46	10.08	12.35	—	11.43	—	11.38	—
CaO	0.05	0.02	0.01	0.00	—	0.00	—	0.01	—
BaO	0.83	1.02	1.26	0.28	—	1.12	—	0.95	—
Na_2O	0.02	0.00	0.01	0.00	—	0.01	—	0.01	—
K_2O	9.73	9.79	9.62	10.11	—	9.68	—	9.48	—
F	0.23	0.20	0.20	0.25	—	0.19	—	0.20	—
Cl	0.07	0.07	0.08	0.10	—	0.03	—	0.05	—
Total.	97.04	97.60	96.86	97.06	—	95.79	—	96.49	—
Si	2.70	2.70	2.70	2.72	—	2.65	—	2.69	—
Al	1.34	1.33	1.34	1.31	—	1.35	—	1.33	—
Ti	0.33	0.33	0.33	0.32	—	0.35	—	0.33	—
Fe	1.16	1.25	1.28	1.06	—	1.16	—	1.18	—
Mn	0.00	0.00	0.01	0.00	—	0.01	—	0.00	—
Mg	1.27	1.18	1.16	1.38	—	1.31	—	1.29	—
Ca	0.00	0.00	0.00	0.00	—	0.00	—	0.00	—
Ba	0.03	0.03	0.04	0.01	—	0.03	—	0.03	—
K	0.94	0.95	0.94	0.96	—	0.95	—	0.92	—
F	0.06	0.05	0.05	0.06	—	0.05	—	0.05	—
Cl	0.01	0.01	0.01	0.01	—	0.00	—	0.01	—
Mg/(Mg + Fe)	52.1	48.7	47.4	56.6	—	53.0	—	52.2	—
					Plagioclase (8 oxygens)				
				host exsol.				host exsol.			
SiO_2	56.95	57.97	58.50	61.96	64.78	56.59	57.88	60.49	64.51	58.84	59.70
Al_2O_3	27.95	27.32	26.84	24.40	18.73	27.69	27.19	25.11	18.17	26.12	25.15
FeO	0.13	0.26	0.09	0.06	0.00	0.21	0.09	0.16	0.06	0.16	0.10
MgO	0.00	0.02	0.01	0.00	0.00	0.01	0.01	0.00	0.02	0.01	0.00
CaO	9.71	9.08	8.22	5.67	0.03	9.69	9.10	6.60	0.04	8.36	7.25
BaO	0.01	0.01	0.01	0.03	1.03	0.00	0.09	0.00	1.81	0.03	0.06
Na_2O	5.87	6.00	6.55	8.13	0.63	5.82	6.15	7.51	0.57	6.48	7.17
K_2O	0.23	0.28	0.29	0.37	15.41	0.24	0.30	0.52	15.06	0.35	0.43
Total	100.85	100.94	100.50	100.62	100.61	100.25	100.81	100.39	100.24	100.35	99.86
Ca	0.46	0.43	0.39	0.27	0.00	0.47	0.43	0.31	0.00	0.40	0.35
Na	0.51	0.52	0.57	0.70	0.06	0.51	0.53	0.65	0.05	0.56	0.62
K	0.01	0.02	0.02	0.02	0.91	0.01	0.02	0.03	0.89	0.02	0.03
Ba	0.00	0.00	0.00	0.00	0.02	0.00	0.00	0.00	0.03	0.00	0.00

Cations and Mg/(Mg + Fe) ratios calculated assuming all Fe as Fe^{2+} (see text for discussion of Fe^{2+}/Fe^{3+} ratios). 'Margin' refers to the boundary between the 'light' and 'dark' domains.

PRESSURE–TEMPERATURE CONDITIONS

Table 4 lists calculated P–T values for the metagabbros. Only equilibria involving garnet, orthopyroxene and clinopyroxene were selected: activity–composition relations are less uncertain for these minerals than for the hydrous minerals biotite and amphibole, and experimental diffusion studies show that cation diffusion is slower in garnet and pyroxenes than in hydrous minerals (Lasaga, 1983), so that these minerals may better record peak P–T conditions. Although during vein formation garnet was unstable with respect to the introduced Na + Si-bearing material, the newly formed pyroxenes and the unreacted garnet appear to have equilibrated (for example, K_d(Fe–Mg) between garnet and pyroxenes in different compositional domains of a given rock are similar).

All the chemical data required for the calculations can be obtained from Table 3. Values in Table 4 are calculated assuming all Fe is Fe^{2+}. The average effects of applying Fe^{2+}/Fe^{3+} corrections are also listed.

Temperature

For temperature estimates, a pressure of 8.0 kbar has been used. Temperatures change by less than 6°C/kbar except for the Harley & Green (1982) Opx–Grt Al_2O_3-solubility thermobarometer, which changes by 21°C/kbar. The two preferred calibrations are the Opx–Cpx calibration of Lindsley (1983) and the Grt–Cpx calibration of Pattison & Newton (1989), both of which are based on large numbers of reversed experiments using crystalline starting materials. Lindsley (1983) warns that his subtraction scheme for 'others' components in the pyroxenes may underestimate the 'Wo' component, resulting in a corresponding overestimate of temperature.

The scatter of calculated temperatures from three different samples of the same rock type highlights the vagaries of exchange thermometry in high-grade rocks, in which down-temperature re-equilibration must be expected to have occurred (e.g. Frost & Chacko, 1989). If variable down-temperature re-equilibration occurred, a minimum estimate of peak temperature can be obtained from the highest of a range of temperatures for a given calibration, assuming equilibrium was attained and the calibration is accurate. Taking this approach for the Grt–Cpx calibration of Pattison & Newton (1989), a minimum peak temperature of 700° C is indicated.

Pressure

For pressure calculations, the Grt–Cpx minimum temperature estimate of 700° C has been used. If peak temperatures were higher, corresponding pressures will also have been higher; pressure corrections for each 100° C higher temperature are listed in Table 4.

The Grt–Opx–Pl–Qtz (Fe) calibrations are favoured over the others because almandine is the main component in the natural garnets and ferrosilite comprises about half the orthopyroxene, so that uncertainties in activity–composition relations are minimized. The Grt–Opx (Fe)

Table 4. P–T conditions.*

	Calibration	Hu1 dark	Hu1 margin	P2-6-2b dark	P2-6-2b margin	Hu15a dark	Avg. Fe^{2+}/Fe^{3+} correction*	Pressure increase/ 100° C
Temperature (°C)†	PN	600	—	680	700	580	−30	—
Grt–Cpx	Kh	650	—	730	750	630	−20	—
	EG	720	—	780	790	700	−20	—
Grt–Opx	HG	730	710	720	670	710	−10	—
	H	660	650	720	740	660	−10	—
	LG2	780	790	860	900	790	−10	—
Cpx–Opx	L	710	—	770	680	670	+20	—
	Kz	660	—	720	690	730	−40	—
Pressure (kbar)‡	NP1 (Mg)	7.6	—	9.2	9.9	7.9	+0.2	+0.3
Grt–Cpx	MEA1 (Mg)	7.8	—	9.0	10.0	8.0	+0.2	+0.6
Pl–Qtz	MEA2 (Fe)	7.9	—	9.1	9.7	8.4	+0.6	+1.6
Grt–Opx	NP2 (Mg)	6.8	7.0	8.1	8.5	7.1	+0.2	+0.5
Pl–Qtz	PC (Mg)	8.6	9.1	8.3	10.0	9.1	+0.2	+0.8
	BWB (Fe)	7.2	7.3	7.7	7.8	7.4	+0.3	+1.1
	PC (Fe)	8.1	8.3	8.5	8.8	8.3	+0.3	+1.3
	MEA3 (Fe)	8.5	8.8	9.0	9.2	8.8	+0.3	+1.4

* All pressures and temperatures calculated assuming all Fe as Fe^{2+} (see text for discussion of Fe^{2+}/Fe^{3+} correction).
† Temperatures calculated for P = 8 kbar, and rounded to the nearest 10° C.
‡ Pressures calculated for T = 700° C, and rounded to the nearest 0.1 kbar.
Calculations: PN = Pattison & Newton (1989); Kh = Krogh (1988); EG = Ellis & Green (1979); HG = Harley & Green (1982); H = Harley (1984); LG2 = Lee & Ganguly (1988), eq. 11.2; L = Lindsley (1983), Cpx limb of solvus; Kz = Kretz (1982), eq. 15; NP1, NP2 = Newton & Perkins (1982), Mg-Cpx and Mg-Opx expressions, modified by Eckert & Newton (1989b,a) respectively; MEA1(Mg), MEA2(Fe), MEA3 = Moecher *et al.* (1988), Mg-Cpx, Fe-Cpx and Fe-Opx expressions respectively; PC (Mg), PC (Fe) = Perkins & Chipera (1985), Mg and Fe expressions; BWB = Bohlen *et al.* (1983).

calibrations show the least scatter of all the methods, even though there are consistent differences between individual calibrations (Table 4). Because quartz is not present in the host metagabbro and some of the diffuse veins, the calculated pressures are maximum estimates. Averaging the three calibrations yields an estimate of 8.2 kbar; for 800° C the corresponding pressure is 9.5 kbar.

Experimentally determined hornblende-breakdown reactions

Figure 9 is a compilation of the limited experimental data available for high-grade reactions involving amphibole, plagioclase, garnet, pyroxenes, quartz, vapour and liquid (sources of data listed in the figure caption). Most of the experimental data are unreversed and a range of bulk compositions is represented. The P–T results from the metagabbros have been plotted as an open-ended box corresponding to an uncertainty of ±1 kbar about the Grt–Opx–Pl–Qtz (Fe) pressures.

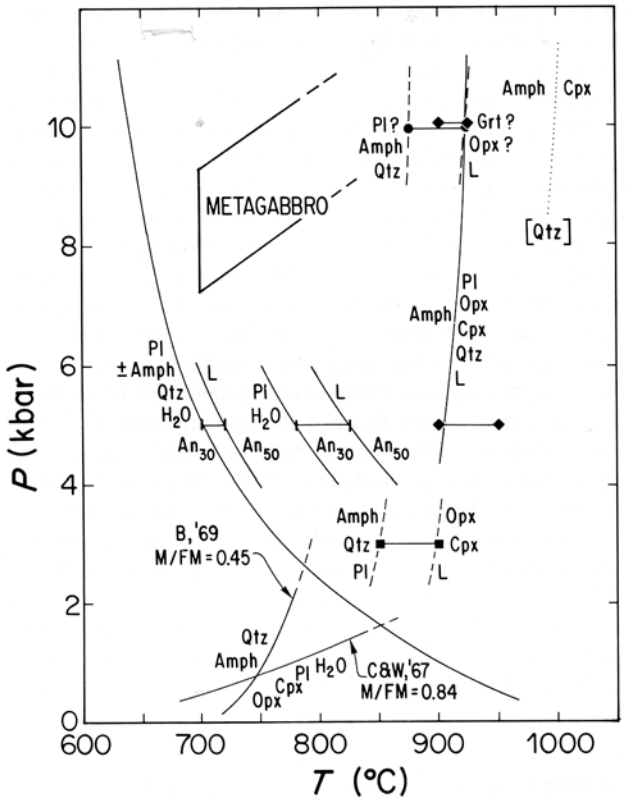

Fig. 9. Summary of available experimental data on hornblende breakdown under vapour-present and vapour-absent conditions, compared to estimated P–T conditions in the net-veined metagabbros (open-ended rhomb). Hbd + Qtz = Opx + Cpx + Pl + H_2O from Choudhuri & Winkler (1967; bulk rock Mg/(Mg + Fe) = 0.84) and Binns (1969; bulk Mg/(Mg + Fe) = 0.45). Pl + Qtz ± Hbd + H_2O = L from Piwinskii (1968). The 5-kbar constraints on Pl + Qtz + H_2O = L (tonalite solidus) and Pl + H_2O = L (anorthosite solidus), for An_{30-50}, from Johannes (1978); the An_{30}-tonalite solidus coincides with the Piwinskii tonalite curve. Square symbol brackets at 3 kbar bound the melting interval of Hbd + Pl + Qtz = Opx + Cpx + L from Beard & Lofgren (1989; Mg/(Mg + Fe) not given). Solid-circle brackets at 10 kbar are for the melting interval of Hbd + Qtz to melt in tonalite of bulk rock Mg/(Mg + Fe) = 0.43 from Rutter & Wyllie (1988; no indication of specific product assemblage given). Solid-diamond brackets (5 & 10 kbar) are for the reaction Tschemakitic amphibole = Pl(An_{100}) + Qtz + Opx + Cpx + L from Ellis & Thompson (1986; CMASH system). The dotted line shows the approximate location of the incoming of clinopyroxene in quartz-absent amphibolite (assumed to be due to hornblende breakdown; Wyllie, 1977).

GENESIS OF THE VEINS

The central mineralogical differences between the veins and the host metagabbro are the development of orthopyroxene, clinopyroxene and plagioclase in the veins at the expense of hornblende and garnet in the host metagabbro. Quartz is present in the intermediate veins and tonalitic leucosomes, but is not present in the host metagabbro.

Evidence for metasomatism in diffuse and intermediate veins

Mass balance analysis based on measured mineral compositions was performed to see whether the gross mineralogical differences between the veins and host metagabbro could be rationalized by closed-system reactions in the metagabbro. The phases used were hornblende, orthopyroxene, clinopyroxene, plagioclase, garnet, SiO_2 and H_2O in the system CaO–(Fe, Mg)O–Al_2O_3–SiO_2–H_2O, using the following simplified mineral formulae based on the analyses in Table 3: (Hbd: $Ca_2(Fe, Mg)_{4.5}Al_2Si_6O_{22}(OH)_2$; Cpx: $Ca(Fe, Mg)Si_2O_6$; Opx: $(Fe, Mg)_2Si_2O_6$; Grt: $Ca_{0.5}(Fe, Mg)_{2.5}Al_2Si_3O_{12}$; Pl: $CaAl_2Si_2O_8$). The only reactions that consume hornblende or hornblende + garnet are the Cpx-absent reaction $4Hbd + 8Grt + 26SiO_2 = 19Opx + 12Pl + 2H_2O$ and the Grt-absent reaction $4Hbd + 10SiO_2 = 4Cpx + 7Opx + 4Pl + 2H_2O$. However, *both* of these reactions require the addition of SiO_2 to proceed. Note that the Qtz-absent reaction Hbd + Opx + Pl = Cpx + Grt + H_2O has orthopyroxene as a reactant and garnet as a product, which contradicts the modal and textural data. These results are in agreement with the whole-rock chemical data, which suggest that the vein mineralogy could not have been produced in a closed system from the quartz-absent host metagabbro.

Using exact mineral compositions and a more complete set of components, including Na_2O and separating FeO and MgO, gives essentially the same results. For example, using the exact mineral formulae in Table 3 for hornblende and garnet from 'Hu1 dark' and for clinopyroxene, orthopyroxene and plagioclase from 'Hu1 light', the garnet-absent reaction is: $0.36Hbd + 1.0SiO_2 + 0.15Na = 0.50Cpx + 0.48Opx + 0.52Pl + 0.16Fe + 0.18H_2O$. To balance the reaction, Na and Si must be introduced and Fe and H_2O liberated. Other model reactions are possible, depending on assumptions about relative mobility of elements.

An alternative explanation for the Si-rich veins is that, prior to vein development, quartz was present as part of a

stable quartz-bearing domain in the metagabbro which was later transformed into the vein assemblage. This appears to be ruled out by the similar composition of the hornblende in the host metagabbro and in the veins, both of which are more Al-rich than hornblende found in typical quartz-bearing hornblende-granulites (e.g. Engel *et al.*, 1964; Hansen *et al.*, 1987).

Another alternative is that the host metagabbro and veins formed from internal differentiation of unveined metagabbro. In this scenario, the veins would represent segregated leucosome and the host metagabbro would represent the more mafic residue. Several lines of evidence argue against this. In contrast to the tonalitic leucosomes, which have several textural features characteristic of segregated leucosomes in anatectic migmatites, the gradational margins and overprinting textures of the diffuse and intermediate veins on the host metagabbro are features unlike those of segregated leucosomes in anatectic migmatites (e.g. Johannes, 1988). Similarities between unveined Type 2 metagabbro and the mafic domains in the net-veined metagabbro, including lack of quartz, similar whole-rock composition, and comparable amphibole composition, give no indication of the formation of a less-siliceous, more-mafic residue that would be required to balance the internal generation of siliceous leucosome. In the diffuse veins, K shows no enrichment relative to the host metagabbro, which would be expected if the leucosomes were anatectic. Many diffuse veins are quartz-absent; based on the few experiments available, extreme temperatures (>900° C) would be required for vapour-absent melting of quartz-absent amphibolite (Fig. 9), and silica-undersaturated assemblages would result (Ellis & Thompson, 1986). Finally, if internal dehydration melting of amphibolite was responsible for the formation of melt and pyroxenes, then upon cooling and crystallization of the melt some degree of rehydration of the pyroxenes might be anticipated; none is seen.

Consequently, open-system behaviour seems a better model. Si, Na, Ba, Sr and possibly Al could have been introduced in a low-a_{H_2O} melt or fluid. The diffuse margins of many of the veins, the occurrence of hornblende and garnet relics in the veins, and the presence of plagioclase moats around garnet and hornblende partially replaced by pyroxenes in the host–vein transition zone are suggestive of subsolidus processes. Similar features are seen in the transecting charnockitic veins and patches in the southern Indian amphibolite–granulite transition, which are interpreted to have been caused by infiltrating CO_2-rich fluids (Newton *et al.*, 1980; Hansen *et al.*, 1984; Stahle *et al.*, 1987). Infiltration by low-a_{H_2O} fluid also provides a means of extracting the water released from hornblende breakdown without rehydrating the pyroxenes. Although the cross-cutting tonalitic leucosomes are suggestive of a melt, these appear to have been derived from within the metagabbro and may be related to the introduction of K along with the other introduced elements.

The introduction of discrete millimetre–centimetre-thick dykelets of dry or CO_2-rich siliceous melt is also a possibility. However, even if such melts were to cause hornblende breakdown immediately adjacent to their margins, their small volume relative to the host metagabbro would mean that relatively little reaction would have to occur before the melts had equilibrated with the host metagabbro. Only if the melts were through-going could substantial reaction proceed in the host metagabbro. Evidence for lack of mobility of such melts in the net-veined rocks is provided by the internally generated tonalitic leucosomes (Fig. 4).

Low-a_{H_2O} fluids

A conspicuous feature of the veins is their anhydrous nature relative to the hornblende-rich host metagabbro. Even at the minimum temperatures indicated by geothermometry, an introduced Si + Na + Ba + Sr ± K ± Al-enriched aqueous fluid phase would result in melting of the metagabbro (mainly the plagioclase fraction) without significant conversion of hornblende to its anhydrous equivalents (pyroxene). Thus, the introduced fluids responsible for the conversion of hornblende ± garnet to pyroxenes + plagioclase must have been low in a_{H_2O}.

Because of uncertainty in activity–composition relations of amphibole, an estimate of a_{H_2O} based on amphibole dehydration equilibria (e.g. Phillips, 1980) has not been attempted. Displacing the tonalite or anorthosite solidus in the *non-ferromagnesian system* due to reduced a_{H_2O}, such that it goes through the metamorphic P–T box (e.g. Newton, 1986), may not be valid, given the experimental data of Holloway (1973), Wendlandt (1981) and Peterson & Newton (1989a) which suggest that CO_2 may *lower* rather than raise the solidus in Mg-bearing and perhaps natural melts (in contrast, see Clemens & Wall, 1981). Typical calculated values for a_{H_2O} in other granulite facies terranes fall mainly in the range 0.1–0.5 (e.g. Phillips, 1980; Valley *et al.*, 1983; Edwards & Essene, 1988), which may be taken as a guide to a_{H_2O} conditions here.

A scenario of progressive metasomatism

The formation of the veins can be explained in a scenario of progressive low-a_{H_2O} metasomatism involving two main stages (Fig. 10).

Stage 1: subsolidus dehydration

In outcrop, the first stage of fluid infiltration is represented by the diffuse veins and patches. Prior to vein development, a_{H_2O} in the host metagabbro must have been in the hornblende stability field (Fig. 10). The first out-of-equilibrium, Si + Na + Ba + Sr-enriched, low-a_{H_2O} fluids that were introduced equilibrated with the host metagabbro by causing breakdown of hornblende ± garnet to produce pyroxenes and plagioclase; the dehydration of hornblende will have internally buffered the introduced fluid to higher a_{H_2O}. The Si introduced by the fluids was fixed in the rock by the production of relatively siliceous pyroxenes from the more aluminous hornblende. Na and

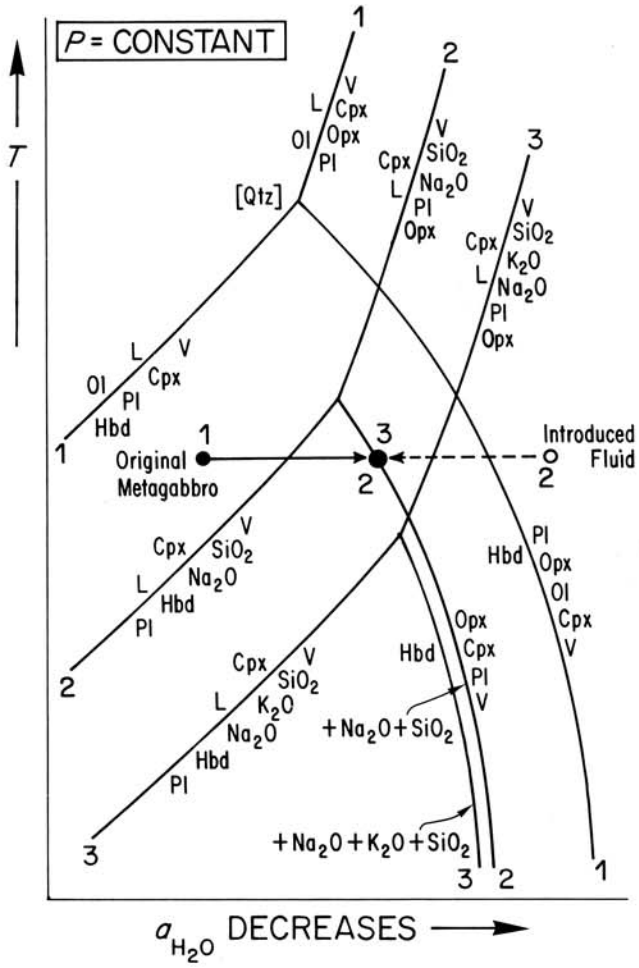

Fig. 10. Schematic T–a_{H_2O} diagram (low-a_{H_2O} portion only) showing possible shifts in melting and dehydration curves for amphibolite due to addition of SiO_2, Na_2O and K_2O. For the melting curves, addition of K and Na expands the stability field of liquid; for the dehydration curve, addition of K and Na expands the stability field of plagioclase, shifting the curve to the left. '1' corresponds to the quartz-absent metagabbro host. Reaction stoichiometries for quartz-absent reactions are uncertain (Ellis & Thompson, 1986). '2' corresponds to infiltration by low-a_{H_2O}, Si + Na-enriched fluids, leading to dehydration by the reaction Hbd + SiO_2 ± Na_2O = Opx + Cpx + Pl + V. '3' corresponds to addition of K along with Na and Si, shifting the solidus so that infiltration of fluid causes melting rather than dehydration.

Ba were fixed in the newly formed plagioclase. The hornblende and garnet in the host metagabbro will have acted as reactant reservoirs, losing their margins to make pyroxenes + plagioclase as infiltration proceeded.

Stage 2: anatexis

The second stage in vein development is represented by the quartz + antiperthitic plagioclase association in the tonalitic leucosomes and intermediate veins. The composition and texture of the tonalitic leucosomes indicate an anatectic origin. The tonalitic leucosomes grade smoothly into the intermediate veins, which suggests that they may be products of the same process taken to different degrees (i.e. the intermediate veins may indicate lower extents of reaction).

The change from conditions conducive for subsolidus dehydration to those conducive for anatexis must have involved a change in P–T or fluid composition. Low-a_{H_2O} conditions still must have prevailed during anatexis because the tonalitic leucosomes contain orthopyroxene and are commonly bordered by orthopyroxene-enriched selvages (Fig. 7).

One possibility is that during fluid infiltration, the temperature rose such that the fluid, rather than causing solid-state dehydration, caused melting (Fig. 10). However, except under P–T–a_{H_2O} conditions close to those appropriate for dehydration melting (equivalent to the invariant points in Figs 1 & 10), this would require a substantial temperature increase. Pressure changes would make only a slight difference (Fig. 9). One process that would *not* explain the observed anatexis is a simple increase in a_{H_2O} in an introduced fluid; a moderate increase in a_{H_2O} (all other conditions being held constant) would result in rehydration of the pyroxenes and plagioclase to hornblende, while a large increase in a_{H_2O} in the introduced fluid would result in the production of water-rich melts (Figs 1 & 10).

A more likely explanation is that the introduction of K along with Na and Si lowered the solidus of quartz-absent amphibolite (Figs 9 & 10). At 5 kbar, plagioclase + quartz + H_2O melts to tonalitic liquid about 100° C lower than plagioclase + H_2O melts (Johannes, 1978). Addition of Na lowers the tonalite solidus further; a change from An_{50} to An_{30} lowers the solidus by about 20° C (Johannes, 1978). The introduction of K further lowers the tonalite solidus, although it is uncertain by how much; at 5 kbar, the separation between An_{30} + Qtz + H_2O = L and An_{30} + Kfs + Qtz + H_2O = L is about 50° C (Johannes, 1980). The positive correlation between the presence of antiperthitic plagioclase, increased whole-rock K and coarseness of the veins suggests that the introduction of K may have been of key importance in promoting anatexis in the metagabbros. In felsic migmatites studied by Olsen (1985) and Johannes (1988), introduction of K was also considered to have been important in the anatectic process.

The non-hydrous volatile component in the fluid may also have been important during anatexis. In other low-a_{H_2O} granulites, this component is considered partly from fluid inclusion evidence and partly by default to be CO_2 (e.g. Touret, 1971; Newton *et al.*, 1980). There is slightly higher CO_2 in the veins than in the host metagabbro. Reversed melting experiments of phlogopite + quartz ± sanidine in mixed H_2O–CO_2 fluids by Peterson & Newton (1989a) suggest that the addition of CO_2 promotes both H_2O-absent and H_2O-consuming melting reactions. Compared to the location of the vapour-absent dehydration-melting reaction Phl + Qtz + San = Opx + L (805° C at 8 kbar), the equivalent reaction with an H_2O–CO_2 fluid of $X_{H_2O} = 0.27$ occurs at 740° C; relative to the H_2O-saturated melting reaction Phl + Qtz + H_2O = Opx + L (785° C at 8 kbar), the equivalent reaction for an H_2O–CO_2 fluid of $X_{H_2O} = 0.5$ is *c.* 760° C.

Taking all of these effects into account, the introduction of (Si, Na, K)-enriched H_2O–CO_2 fluids can lower the solidus of quartz-absent amphibolite substantially. In Fig. 10, the change from infiltration-driven dehydration (2) to infiltration-driven melting (3) is represented by the lowering of the tonalite solidus due to introduction of K. In contrast to the dehydration stage, in which pyroxenes + plagioclase were produced at the expense of hornblende ± garnet in the host metagabbro, it may be that the melting stage involved primarily the quartzo-feldspathic component of the rock; this is suggested by the leucocratic compositions of the leucosomes, the smooth transition between the tonalitic leucosomes and the plagioclase ± quartz-rich intermediate veins, and the sharp margins of the leucosomes against the diffuse veins and host metagabbro (Fig. 4).

Cause of changes in fluid composition

The evidence for K-enrichment accompanying anatexis may indicate that the *externally introduced fluids* became more K-rich. Alternatively, the introduced Stage 1 fluid may have become depleted in Si & Na and enriched in K & H_2O due to the breakdown of hornblende ± biotite. These *internally modified fluids*, although not capable on their own of causing anatexis (otherwise they would have caused anatexis in the rock from which they were derived), may have moved and interacted in another part of the rock with the introduced (Si, Na)-bearing fluids, producing a fluid capable of causing anatexis.

Source and introduction of fluids

The source of the fluids is unknown. The net veins in several bodies were flattened and folded prior to incorporation in the enclosing gneiss, so that the fluids could not have originated from the enclosing gneisses. No marble, calc-silicate or graphitic rocks as possible sources of CO_2 are found nearby. Charnockitic bodies, suggested by Frost & Frost (1987) to be possible sources for CO_2-rich fluids, occur sporadically in the vicinity (Nadeau, 1985). However, the gneissic fabric of the charnockite suggests that it may pre-date the metagabbro, which is confirmed elsewhere in the Seguin subdomain by a 1500–1400-Ma age range for charnockitic gneiss compared to *c.* 1170-Ma coronitic metagabbro. Unexposed deep-seated sources, such as mantle-derived fluids (Wyllie & Huang, 1976) or fluids released from a basaltic underplate (Touret, 1971), remain a possibility. Fluid inclusion and stable isotope data are needed to provide further constraints on fluid origin.

The method by which the fluids were channellized through relatively homogeneous metagabbro is also uncertain. One possibility is that the fluids were channellized through pre-existing fractures in the metagabbro, such as proposed by Bradshaw (1989) for infiltration-induced veins in granulites from Fiordland, New Zealand. Bradshaw demonstrated that there was a net volume reduction during vein-formation, which facilitated further incursion of fluids. If SiO_2 had been present in the host metagabbro as quartz, the vein-forming reactions would likewise have resulted in a negative volume change; however, because SiO_2 was introduced in a fluid phase and fixed in the rock by reaction with the host metagabbro, there was an increase in mass and a corresponding increase in volume of solids in the veins. Consequently, it appears that some other mechanism was required.

ACKNOWLEDGEMENTS

I would like to thank A. Davidson for originally sparking my interest in these outcrops during the 'Granulites and Granulites' field trip preceding the 1986 Geological Association of Canada–Mineralogical Association of Canada annual meeting in Ottawa. Thanks are due to B. Hensen for organizing an excellent International Geological Correlation Program, Project 235, field conference in Alice Springs and Sydney, Australia in July 1989, where these results were presented. Reviews by T. Chacko, A. Davidson, E. Essene, J. Percival and R. Newton improved the manuscript substantially. All errors or misconceptions are my own. I acknowledge the help of J. Machacek and R. Walker with the electron microprobe, M. Stout with the point counting, P. Michael with the XRF analysis and R. Davidson for bulk-rock C- and S-analyses. This research was supported by NSERC operating grant no. 037233.

REFERENCES

Albee, A. L. & Ray, L., 1970. Correction factors for electron microprobe microanalysis of silicates, oxides, carbonates, phosphates and sulfates. *Journal of Analytical Chemistry*, **42**, 1408–1414.

Beard, J. S. & Lofgren, G. E., 1989. Melt-forming reactions in amphibolites under water-saturated and fluid-absent (dehydration) melting conditions. *EOS*, **70**, 1395 (abstract).

Bence, A. E. & Albee, A. L., 1968. Empirical connection factors for the electron microanalysis of silicates and oxides. *Journal of Geology*, **76**, 382–403.

Binns, R. A., 1969. Hydrothermal investigation of the amphibolite–granulite facies boundary. *Special Publication of the Geophysical Society of Australia*, **2**, 341–344.

Bohlen, S. R., Wall, V. J. & Boettcher, A. L., 1983. Experimental investigation and application of garnet-granulite equilibria. *Contributions to Mineralogy and Petrology*, **83**, 52–61.

Bradshaw, J. Y., 1989. Early Cretaceous vein-related garnet granulite in Fiordland, Southwest New Zealand: a case for infiltration of mantle-derived, CO_2-rich fluids. *Journal of Geology*, **97**, 697–717.

Choudhuri, A. & Winkler, G. F., 1967. Anthophyllit und Hornblend in einigen metamorphen Reaktionen. *Contributions to Mineralogy and Petrology*, **14**, 293–315.

Clemens, J. D. & Wall, V. J., 1981. Origin and crystallisation of some peraluminous (S-type) granitic magmas. *Canadian Mineralogist*, **19**, 111–131.

Davidson, A. & van Breeman, O., 1988. Baddeleyite–zircon relationships in coronitic metagabbro, Grenville Province, Ontario: implications for geochronology. *Contributions to Mineralogy and Petrology*, **100**, 291–299.

Davidson, A., Culshaw, N. G. & Nadeau, L., 1982. A tectono-metamorphic framework for part of the Grenville Province, Ontario. In: *Studies in the Grenville Province.*

Current Research, Part A, Paper 82–1*A* (eds Davidson, A., Nadeau, L., Grant, S. M. & Pryer, L. L.), pp. 139–145. Geological Survey of Canada.

Davidson, A. & Grant, S. M., 1986. Reconnaissance geology of western and central Algonquin Park and detailed study of coronitic olivine metagabbro, Central Gneiss Belt, Grenville Province of Ontario. In: *Studies in the Grenville Province. Current Research, Part B, Paper* 86-1*B* (eds Davidson, A., Nadeau, L., Grant, S. M. & Pryer, L. L.), pp. 837–848. Geological Survey of Canada.

Eckert, J. O. & Newton, R. C., 1989a. Re-calibration of the garnet–orthopyroxene geobarometer by oxide-melt solution calorimetry of stoichiometric mineral mixes. *EOS*, **70,** 493.

Eckert, J. O. & Newton, R. C., 1989b. Recalibration of the garnet–anorthite–diopside–quartz (GADS) geobarometer by oxide-melt solution calorimetry of stoichiometric mineral mixes. *EOS*, **70,** 1392.

Edwards, R. L. & Essene, E. J., 1988. Pressure, temperature and C–O–H fluid fugacities across the amphibolite–granulite transition, Northwest Adirondack Mountains, New York. *Journal of Petrology*, **29**, 39–72.

Ellis, D. J. & Green, D. J., 1979. An experimental study of the effect of Ca upon garnet–clinopyroxene Fe–Mg exchange equilibria. *Contributions to Mineralogy and Petrology*, **71,** 13–22.

Ellis, D. J. & Thompson, A. B., 1986. Subsolidus and partial melting reactions in the quartz-excess $CaO + MgO + Al_2O_3 + SiO_2 + H_2O$ system under water-excess and water-deficient conditions to 10 kb: some implications for the origin of peraluminous melts from mafic rocks. *Journal of Petrology*, **27,** 91–121.

Engel, A. E. J., Engel, C. G. & Havens, R. G., 1964. Mineralogy of amphibolite interlayers in the gneiss complex, northwest Adirondacks. *Journal of Geology*, **72,** 131–156.

Friend, C. R. L., 1981. Charnockite and granite formation and influx of CO_2 at Kabbaldurga. *Nature*, **294,** 550–552.

Friend, C. R. L., 1983. The link between charnockite formation and granite production: evidence from Kabbaldurga, Karnataka, Southern India. In: *Migmatites, Melting and Metamorphism* (eds Atherton, M. P. & Gribble, C. D.), pp. 264–276. Shiva, Nantwich.

Frost, B. R. & Chacko, T., 1989. The granulite uncertainty principle: limitations on thermobarometry in granulites. *Journal of Geology*, **97,** 425–450.

Frost, B. R. & Frost, C. D., 1987. CO_2, melts and granulite metamorphism. *Nature*, **327,** 503–506.

Grant, J. A., 1985. Phase equilibria in partial melting of pelitic rocks. In: *Migmatites* (ed. Ashworth, J. R.), pp. 86–144. Blackie, Glasgow.

Grant, J. A., 1986. Quartz–phlogopite–liquid equilibria and origins of charnockites. *American Mineralogist*, **71,** 1071–1075.

Grant, S. M., 1987. The petrology and structural relations of metagabbros, southwestern Grenville Province, Canada. *Unpubl. PhD Thesis, University of Leicester*, 208 pp.

Grant, S. M., 1988. Diffusion models for corona formation in metagabbros from the Western Grenville Province, Canada. *Contributions to Mineralogy and Petrology*, **98,** 49–63.

Greenwood, H. J., 1975. The buffering of pore fluids by metamorphic reactions. *American Journal of Science* **275,** 573–593.

Hansen, E. C., Janardhan, A. S., Newton, R. C., Prame, W. K. B. N. & Ravindra Kumar, G. R., 1987. Arrested charnockite formation in southern India and Sri Lanka. *Contributions to Mineralogy and Petrology*, **96,** 225–244.

Hansen, E. C., Newton, R. C. & Janardhan, A. S., 1984. Fluid inclusions in rocks from the amphibolite-facies gneiss to charnockite progression in Southern Karnataka, India: direct evidence concerning the fluids of granulite metamorphism. *Journal of Metamorphic Geology*, **2,** 249–264.

Harley, S. L., 1984. Experimental calibration of Fe–Mg exchange between garnet and orthopyroxene and its use as a geothermometer. *Contributions to Mineralogy and Petrology*, **86,** 359–373.

Harley, S. L. & Green, D. H., 1982. Garnet–orthopyroxene barometry for granulites and peridotites. *Nature*, **300,** 697–701.

Holloway, J. R., 1973. The system pargasite–H_2O–CO_2: a model for melting of a hydrous mineral with a mixed-volatile fluid. I. Experimental results to 8 kbar. *Geochimica et Cosmochimica Acta*, **37,** 651–666.

Johannes, W., 1978. Melting of plagioclase in the systems Ab–An–H_2O and Qz–Ab–An–H_2O at $PH_2O = 5$ kbar, an equilibrium problem. *Contributions to Mineralogy and Petrology*, **66,** 295–303.

Johannes, W., 1980. Metastable melting in the granite system Qz–Or–Ab–An–H_2O. *Contributions to Mineralogy and Petrology*, **72,** 73–80.

Johannes, W., 1983. On the origin of layered migmatites. In: *Migmatites, Melting and Metamorphism* (eds Atherton, M. P. & Gribble, C. D.), pp. 234–248. Shiva, Nantwich.

Johannes, W., 1988. What controls partial melting in migmatites? *Journal of Metamorphic Geology*, **6,** 451–465.

Kretz, R., 1982. Transfer and exchange equilibria in a portion of the pyroxene quadrilateral as deduced from natural and experimental data. *Geochimica et Cosmochimica Acta*, **46,** 411–422.

Krogh, E. J., 1988. The garnet–clinopyroxene Fe–Mg geothermometer—a reinterpretation of existing experimental data. *Contributions to Mineralogy and Petrology*, **99,** 44–48.

Lamb, W. M. & Valley, J. W., 1984. Metamorphism of reduced granulites in low-CO_2 vapor-free environment. *Nature*, **312,** 56–58.

Lasaga, A. C., 1983. Geospeedometry: an extension of geothermometry. In: *Advances in Geochemistry*, Vol. 3 (ed. Saxena, S. K.), pp. 81–114. Springer-Verlag, Berlin.

Leake, B. E., 1978. Nomenclature of amphiboles. *American Mineralogist* **63,** 1023–1052.

Lee, H. Y. & Ganguly, J., 1988. Equilibrium compositions of coexisting garnet and orthopyroxene: experimental determinations in the system FeO–MgO–Al_2O_3–SiO_2, and applications. *Journal of Petrology*, **29,** 93–113.

Lindsley, D. H., 1983. Pyroxene thermometry. *American Mineralogist*, **68,** 477–493.

Mehnert, K. R., 1968. *Migmatites and the Origin of Granitic Rocks*. Elsevier, Amsterdam.

Moecher, D. P., Essene, E. J. & Anovitz, L. M., 1988. Calculation and application of clinopyroxene–garnet–plagioclase–quartz geobarometers. *Contributions to Mineralogy and Petrology*, **100,** 92–106.

Nadeau, L., 1985. Characterization of lithotectonic units and their boundaries in the Huntsville region, Central Gneiss Belt. In: *Studies in the Grenville Province. Current Research, Part A, Paper* 85-1*A* (eds Davidson, A., Nadeau, L., Grant, S. M. & Pryer, L. L.), pp. 464–474. Geological Survey of Canada.

Newton, R. C., 1986. Petrologic aspects of Precambrian granulite facies terrains bearing on their origins. In: *Proterozoic Lithosphere Evolution* (ed. Kroner, A.) *American Geophysical Union Geodynamics Series*, **17,** 11–26.

Newton, R. C. & Perkins, D. III, 1982. Thermodynamic calibration of geobarometers based on the assemblages garnet–plagioclase–orthopyroxene–(clinopyroxene–) quartz. *American Mineralogist*, **67,** 203–222.

Newton, R. C., Smith, J. V. & Windley, B. F., 1980. Carbonic metamorphism, granulites and crustal growth. *Nature*, **288,** 45–50.

Nicholls, J. & Stout, M. Z., 1986. Electron beam analytical instruments and the determination of modes, spatial variations of minerals and textural features of rocks in polished section. *Contributions to Mineralogy and Petrology*, **94,** 395–404.

Nicholls, J. & Stout, M. Z., 1988. Picritic melts in Kilauea—evidence from the 1967–1968 Halemaumau and Hiiaka eruptions. *Journal of Petrology*, **29,** 1031–1057.

Olsen, S. N., 1985. Mass balance in migmatites. In: *Migmatites* (ed. Ashworth, J. R.), pp. 145–179. Blackie, Glasgow.

Papike, J. J., Cameron, K. L. & Baldwin, K., 1974. Amphiboles

and pyroxenes: characterisation of OTHER than quadrilateral components and estimates of ferric iron from microprobe data. *Geological Society of America, Abstracts with Programs*, **6**, 1053–1054.

Pattison, D. R. M. & Newton, R. C., 1989. Reversed experimental calibration of the garnet–clinopyroxene Fe–Mg exchange thermometer. *Contributions to Mineralogy and Petrology*, **101**, 87–103.

Perkins, D. III. & Chipera, S. J., 1985. Garnet–orthopyroxene–plagioclase–quartz barometry: refinement and application to the English River subprovince and the Minnesota River Valley. *Contributions to Mineralogy and Petrology*, **89**, 69–80.

Peterson, J. W. & Newton, R. C., 1989a. CO_2-enhanced melting of biotite-bearing rocks at deep-crustal pressure–temperature conditions. *Nature*, **340**, 378–380.

Peterson, J. W. & Newton, R. C., 1989b. Reversed experiments on biotite–quartz–feldspar melting in the system KMASH: implications for crustal anatexis. *Journal of Geology*, **97**, 465–485.

Phillips, G. N., 1980. Water activity changes across an amphibolite–granulite facies transition, Broken Hill, Australia. *Contributions to Mineralogy and Petrology*, **75**, 377–386.

Piwinskii, A. J., 1968. Experimental studies of igneous rock series: central Sierra Nevada Batholith, California. *Journal of Geology*, **76**, 548–570.

Powell, R., 1983. Processes in granulite facies metamorphism. In: *Migmatites, Melting and Metamorphism* (eds Atherton, M. P. & Gribble, C. D.), pp. 127–139, Shiva, Nantwich.

Robinson, P., Spear, F. S., Schumacher, J. C., Laird, J., Klein, C., Evans, B. W. & Doolan, B. L., 1982. Phase relations of metamorphic amphiboles: natural occurrence and theory. In: *Amphiboles: Petrology and Experimental Phase Relations* (eds Veblen, D. R. & Ribben, P. H.), *Mineralogical Society of America Reviews in Mineralogy*, **96**, 1–228.

Rutter, M. J. & Wyllie, P. J., 1988. Melting of vapour-absent tonalite at 10 kbar to simulate dehydration-melting in the deep crust. *Nature*, **331**, 159–160.

Sevigny, J. H., 1987. Geochemistry of Late Proterozoic amphibolites and ultramafic rocks, southeastern Canadian Cordillera. *Canadian Journal of Earth Sciences*, **25**, 1323–1337.

Stahle, H. J., Raith, M., Hoernes, S. & Delfs, A., 1987. Element mobility during incipient granulite formation at Kabbaldurga, Southern India. *Journal of Petrology*, **28**, 803–834.

Thompson, A. B., 1982. Dehydration melting of pelitic rocks and the generation of H_2O-undersaturated granitic liquids. *American Journal of Science*, **282**, 1567–1595.

Touret, J., 1971. Le facies granulite en Norvege meridionale. 2. Les inclusions fluides. *Lithos*, **4**, 423–436.

Valley, J. W., McLelland, J., Essene, E. J. & Lamb, W., 1983. Metamorphic fluids in the deep crust: evidence from the Adirondacks. *Nature*, **301**, 226–228.

Waters, D. J., 1988. Partial melting and the formation of granulite facies assemblages in Namaqualand, South Africa. *Journal of Metamorphic Geology*, **6**, 387–404.

Wendlandt, R. F., 1981. Influence of CO_2 on melting model granulite facies assemblages: a model for the genesis of charnockites. *American Mineralogist*, **66**, 1164–1174.

Wyllie, P. J., 1977. Crustal anatexis: an experimental overview. *Tectonophysics*, **43**, 41–71.

Wyllie, P. J. & Huang, W. L., 1976. Carbonation and melting reactions in the system $CaO–MgO–SiO_2–CO_2$ at mantle pressures with geophysical and petrological applications. *Contributions to Mineralogy and Petrology*, **54**, 79–107.

Received 20 January 1990; revision accepted 29 April 1990.